Thermal conductivity of $La_{3-x}R_xS_4$ R=Sm, Yb, and Eu

by

George Bailey Kokos

A Thesis Submitted to the

Graduate Faculty in Partial Fulfillment of the

Requirements for the Degree of

MASTER OF SCIENCE

Department: Material Science and Engineering
Major: Metallurgy

1988

TABLE OF CONTENTS

LIST OF TABLES

LIST OF FIGURES

ABSTRACT

The thermal diffusivity values of $La_{2.7}Eu_{0.3}S_4$, $La_{2.2}Eu_{0.8}S_4$, $La_{2.7}Sm_{0.3}S_4$, $La_{2.3}Sm_{0.7}S_4$, $La_{2.7}Yb_{0.2}S_4$, and $La_{2.2}Yb_{0.7}S_4$ were measured by the flash diffusivity method from 400 °C to 1000 °C. These values ranged from .007 cm^2/s to .018 cm^2/s. The thermal conductivities of the ternary rare earth sulfides were calculated from the thermal diffusivity data and ranged from 10.7 mW/cm°C to 31.6 mW/cm°C. The thermal diffusivity values of three thermal conductivity standards (armco iron, NBS graphite, and NBS austenitic stainless steel) obtained using the flash diffusivity apparatus agreed with the accepted values within a deviation of ±10%. Of the ternary rare earth sulfides measured, $La_{2.2}Eu_{0.8}S_4$ had the highest figure of merit at 1000 °C of .525. All these samples had an oxysulfide present at the grain boundaries which degraded their high temperature thermoelectric performance.

INTRODUCTION

There is a need for a reliable, efficient, long life, and low cost thermoelectric material to generate power in radioisotope thermoelectric generators (RTGs). These RTGs have been successfully utilized in the NASA Pioneer and Voyager spacecrafts. Electrical power was provided for long time periods to gather an immense amount of new scientific information about space and the planets. Our space program has demonstrated the usefulness of thermoelectric power as evident by the success of these probes.

A radioactive isotope such as plutonium-238 or strontium-90 acts as a heat source which supplies a constant temperature difference across the thermoelements of a generating device.[1] Currently SiGe is being used in RTGs to convert the heat gradient into electrical power for space exploration. RTGs using SiGe thermoelements produce only a few hundred watts of electrical energy while the power demand is now increasing to the order of kilowatts. Also it must be noted that SiGe is only 5% efficient in converting the heat into electricity, resulting in a cost of $20,000 per electrical watt.[2] This means that thousands of dollars can be saved by increasing the efficiency a few percent. Therefore, it is important to utilize new thermoelectric materials to meet expected increased power requirements more efficiently.

This thesis outlines research to measure the thermal diffusivity of several rare earth sulfides of the form $La_{3-x}R_xS_4$ where R is Yb, Sm, or Eu. These rare earth chalcogenides are important thermoelectric materials due to their high melting points, self-doping capabilities, and low thermal conductivities. These materials are expected to have a thermal conductivity which is much smaller than SiGe.

The operating temperature of the RTG in space is 1000 °C to 1200 °C. A RTG should operate at the highest possible temperature to maximize Carnot efficiency. The power output of SiGe maximizes at 800 °C, but Seebeck coefficient, S, and electrical resistivity, ρ, data of $La_{3-x}Yb_xS_4$, $La_{3-x}Sm_xS_4$, and $La_{3-x}Eu_xS_4$ systems suggest that their power outputs continue to increase above 800 °C.[3]

The power factor (S^2/ρ) at 1000 °C for the n-type and p-type SiGe materials is much greater (19-21 $\mu W/°C^2cm$) than for the rare earth sulfides (3-12 $\mu W/°C^2cm$) as shown in Figure 1.[3] SiGe thermoelements currently being used in RTGs exhibit power factors up to 30 $\mu W/°C^2cm^4$. This is due to the high Seebeck coefficient of the SiGe alloys as shown in Figure 2. The higher electrical resistivity of the ternary rare earth sulfides also decreases their power factor as shown in Figure 3. A maximum power factor (S^2/ρ) at 1000 °C was found for the x=.3 composition, but when a reasonable estimate of the thermal conductivity is made

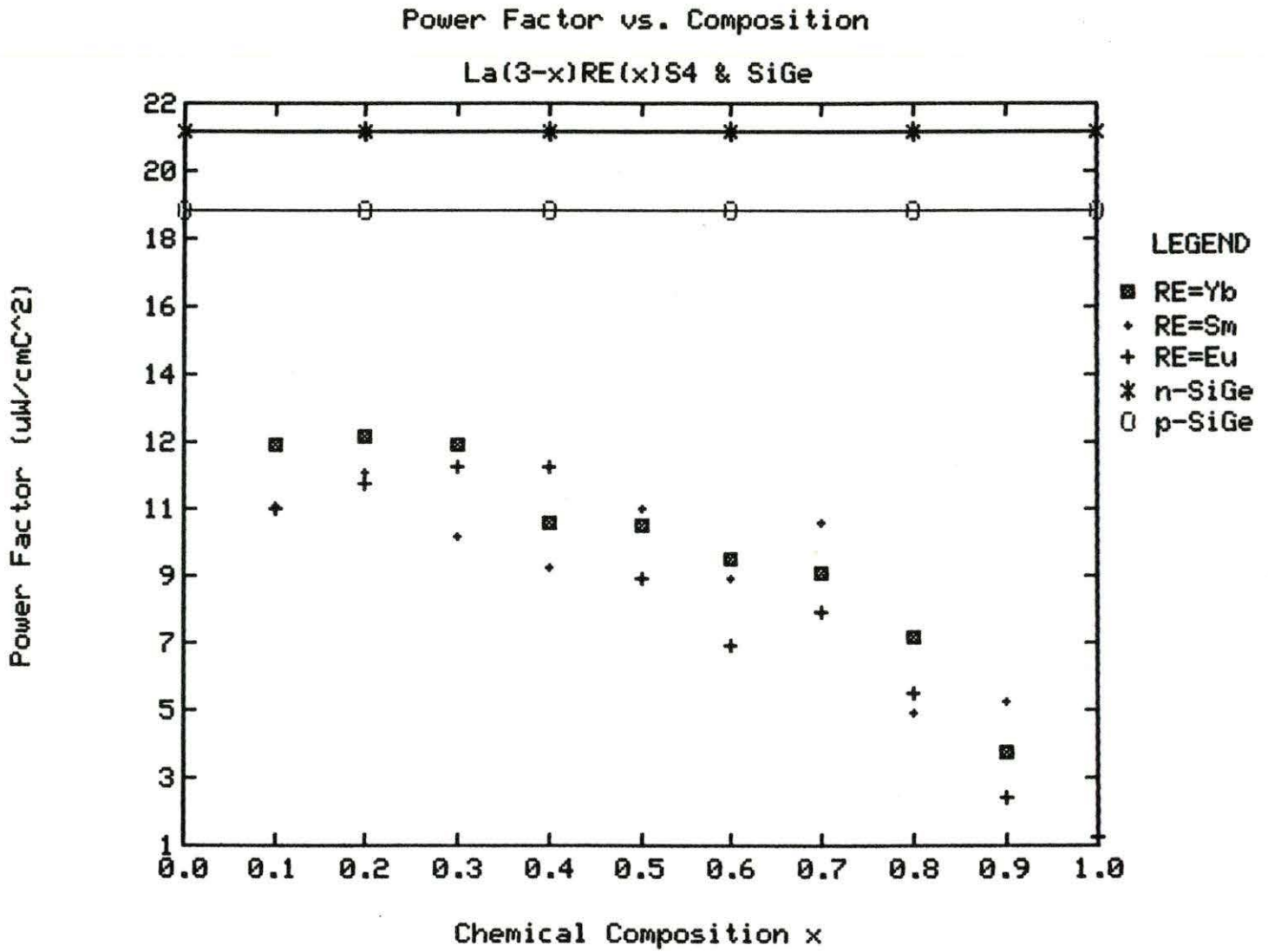

Figure 1. Power factor versus composition for the ternary rare earth sulfides and SiGe alloys

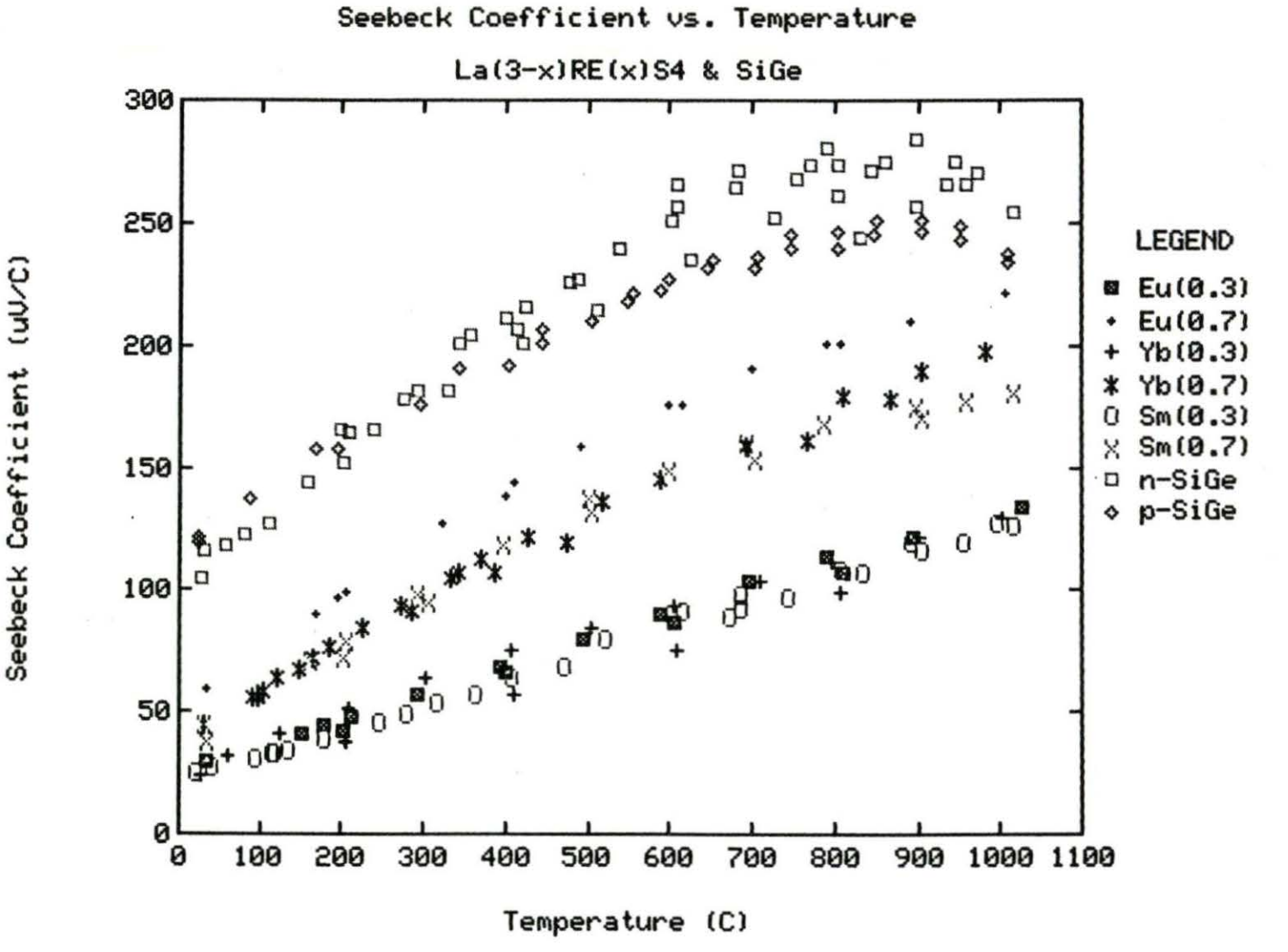

Figure 2. Seebeck coefficient versus temperature for the ternary rare earth sulfides and SiGe alloys

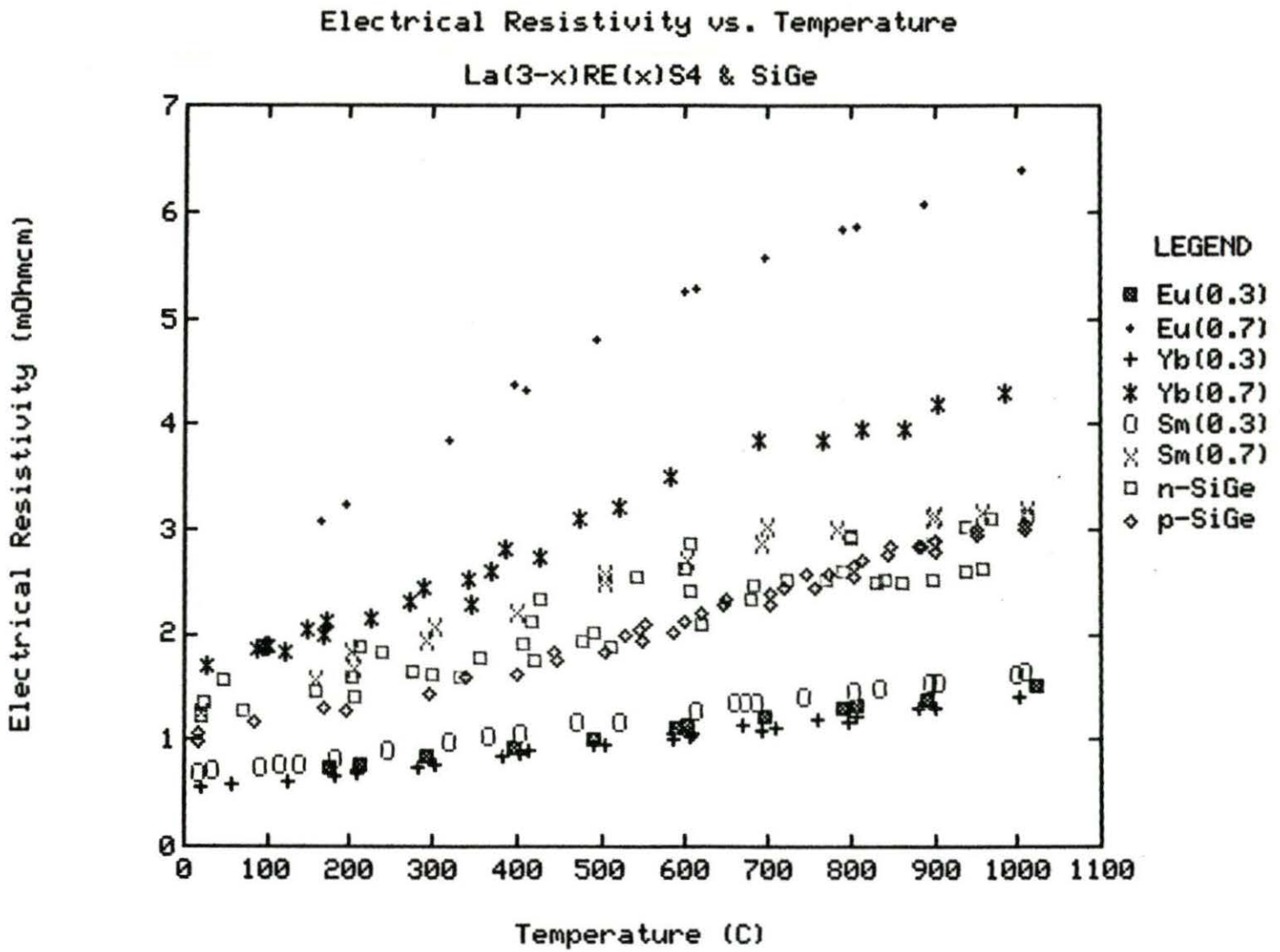

Figure 3. Electrical resistivity versus temperature for the ternary rare earth sulfides and SiGe alloys

for these alloys at 1000 °C (15 mW/cm K)[5] the maximum figure of merit shifts to larger x values such as x=.8. At 1000 °C, the figure of merit could be as high as 0.8 $°C^{-1}$ using 15 mW/cmK^5 as the thermal conductivity. This value is comparable to the figure of merit for the SiGe alloys (.7-.8)[4] currently being used in RTGs. The figure of merit of the ternary rare earth sulfides may keep increasing above 800 °C while that of SiGe decreases. Accurate thermal conductivity data are needed to assess rare earth sulfides as possible next generation thermoelectric elements.

The usefulness of a material for thermoelectric conversion depends upon the material's figure of merit:[6]

(1) $Z = S^2/\rho k$ where Z = Figure of Merit (1/°C)
S = Seebeck Coefficient (μV/°C)
ρ = Electrical Resistivity (mΩcm)
k = Thermal Conductivity (mW/cm°C)

As Z increases to infinity, the efficiency of the thermoelectric system approaches that of an ideal Carnot engine. The Seebeck coefficient and electrical resistivity of the ternary rare earth sulfides have already been measured[4], however thermal conductivity data do not exist for these materials.

To maximize the figure of merit, the thermal conductivity should be minimized. Two major factors affect the thermal

conductivity: a lattice and a carrier contribution. The lattice thermal conductivity can be reduced by employing a small grain size material. This reduction is due to phonon-grain boundary scattering. The short wavelength phonons are scattered by alloy disorder and the long wavelength phonons by grain boundary and second phase effects[7,8,9]. The alloy disorder is most pronounced when the constituent elements have large differences in atomic mass.[1] This is evident when observing the atomic mass of rare earths (138.9 g to 174.9 g) versus the atomic mass of sulfur (32 g). If a material has many carriers present, these electrons carry heat and scatter phonons. The heating effect dominates and raises the thermal conductivity. Therefore, an optimum thermoelectric material will have a very small grain size and a low electron concentration.

Determination of high temperature thermal conductivity is experimentally difficult, because it involves the measurement of heat fluxes that are difficult to control and measure accurately. An easier calculation of the thermal conductivity may be accomplished by measurements of the thermal diffusivity, specific heat, and density. These four quantities are related by the equation:[1]

(2) $k = \alpha C d$ where k = Thermal Conductivity (mW/cm°C)
α = Thermal Diffusivity (cm^2/s)
C = Specific Heat (J/g°C)
d = Density (g/cm^3)

The thermal diffusivity which involves the recording of the time dependence of temperature on the back face of a sample due to a transient thermal disturbance at the front specimen boundary is simple to measure experimentally with the flash diffusivity apparatus. The other two thermophysical properties involved, specific heat and density, are either known or may be measured without difficulty. The heat contents of $La_2S_3(\alpha)$, $La_2S_3(\gamma)$, La_3S_4, and $La_{2.65}Eu_{0.35}S_4$ have been determined by Amano et al.[10] using an adiabatic copper block drop calorimeter[11]. These authors[10] showed that the heat capacities can be calculated for any of the close related ternary rare earth sulfides, because the thermodynamic properties of these alloys do not vary significantly. The density at various temperatures may be calculated from the density at room temperature obtained by x-ray diffraction and the volume coefficient of expansion.

FLASH DIFFUSIVITY METHOD

There are several methods available for measurement of thermal conductivity: steady state, comparator, and dynamic or nonsteady methods. In steady state methods, the temperature gradient is measured under steady state conditions when a known heat flux passes through the sample. Radiant heat losses may be large in comparison with the heat being conducted along the sample, because thermoelectric materials are generally poor conductors of heat. In the comparator technique, disc shaped samples of unknown thermal conductivity are sandwiched between discs of known thermal conductivity and the temperature gradient in the unknown disc and the standards is measured. This method works quite well for measurements on thermoelectric materials. Nonsteady methods help to eliminate radiation effects. One nonsteady state technique is called the Angstrom method in which a periodic heat input is supplied to one end of a bar shaped specimen and the attenuation of the resulting temperature wave is measured. Another nonsteady state technique is called the flash or pulse diffusivity method. It has been chosen the optimum technique for this research.[1,12]

The laser pulse technique has been the most popular technique for determining the thermal diffusivity in the middle 1970's, approximately 80% of the published papers have used this technique. The popularity of this method is due to the ease with

which initial and boundary conditions can be reproduced in a physical experiment.[12] In a study in 1973, Angstrom and electron beam techniques yielded deviations of ±35% for thermal diffusivity data of austenitic stainless steel, while the scatter was within an acceptable band of ±5% utilizing the flash diffusivity method[13].

Parker et al.[14] developed the flash method in 1961 to eliminate the inability to satisfy boundary conditions. Two boundary conditions in particular caused difficulties in the classical techniques: thermal contact resistance between the sample and heat sources and surface heat losses. Thermal contact resistance problems were eliminated by using a flash tube. The flash diffusivity method eliminated heat loss resistance problems by taking measurements in short times such that little cooling took place. Parker determined the thermal diffusivity of metals at room temperature and 135 °C, but it was thought that measurements could be taken at any temperature on all types of materials utilizing the flash method.[14]

Parker's apparatus consisted of a flash lamp, sample holder, chromel-alumel thermocouple, preamplifier, oscilloscope, and Polaroid land camera. The flash lamp, 1 cm from the sample, provided 400 J of energy to heat the sample in the ceramic holder. An intrinsic thermocouple (thermocouple whose individual

wires are joined separately to the sample instead of being joined together to form a bead which is attached to the sample) pressed against the rear face provided a voltage that was amplified, displayed on an oscilloscope, and photographed with a Polaroid land camera.[14]

The ceramic sample holder was opaque, of low thermal conductivity, of exceptional strength, and capable of withstanding thermal shock. This holder was capable of supporting samples as large as 19 mm in diameter and 5 mm thick with spring wire retainers. The intrinsic thermocouple was clamped in a small pin vise and connected to a cold junction plug. The 135 °C experiments were obtained with the aid of an infrared lamp. Thermal equilibrium was checked via the thermocouple output.[14]

The flash diffusivity technique has many advantages. Thermal diffusivity measurements take less than two seconds to complete. Because of the small mass of heater and sample, the ambient temperature can be rapidly changed, thus thermal diffusivity measurements can be taken over a wide temperature range in several hours. In the flash diffusivity technique, the sample is so small, 1 mm to 4 mm, that the boundary condition of initial uniform temperature is satisfied. Thermal diffusivity measurements have been taken at temperatures ranging from 100 K

to 2500 K utilizing this method. The pulse method is applicable to opaque solids[15], liquids[16,17], inorganic materials[18], and anisotropic materials[19]. Translucent materials and coatings[20], temperature-sensitive materials[21], and composites[22,23] must be measured in a layered arrangement [24,25,26,27].

Another advantage of the flash diffusivity method is its precision in calculating the thermal diffusivity, because measurement errors are negligible and nonmeasurement errors may be corrected. These errors are discussed in more detail at the end of the next section.

THEORY

The flash diffusivity method consists of the absorption of a short burst (<1 ms) of radiant energy from a laser or xenon flash lamp on the front surface of a specimen. The resulting temperature-time curve of the back surface is recorded and the thermal diffusivity values are computed using this curve. This curve may be described as a function of time by the equation as derived by Carslaw and Jaeger[28]:

$$(3) \qquad V = \frac{T_m}{T_{L,t}} = 1 + 2\Sigma(-1)^n \exp\left(-\frac{n^2\pi^2\alpha t}{L^2}\right)$$

Where V = Fraction of the maximum temperature rise
T_m = Maximum temperature (°C)
$T_{L,t}$ = Temperature at some length, l, after some time, t, (°C)
n = Number of terms
α = Thermal Diffusivity (cm^2/s)
t = Time (s)
L = Thickness of sample (cm)

The thermal diffusivity may be solved by using a sufficient number of terms in equation 3. Note that the exact amount of the temperature rise or the energy absorbed need not be known. Thus, the thermal diffusivity of a material may be determined from the sample thickness and the time at different normalized temperature values.

Parker et al.[14] suggested a method of determining the thermal diffusivity from the temperature versus time plot. From

the first term of equation 3, he noted that when V=.5 the following formula can be derived.

$$(4) \qquad \alpha_{1/2} = \frac{1.38\ L^2}{\pi^2\ t_{1/2}}$$

Where $\alpha_{1/2}$ = Thermal diffusivity at 1/2 maximum temperature (cm^2/s)
L = Sample thickness (cm)
$t_{1/2}$ = Time to reach 1/2 maximum temperature (s)

The derivation of this formula is shown in Appendix 1. Even though it has been used exclusively in literature, this formula is not a unique point. Any other choice of V would result a different constant in equation 4. If the thermal diffusivity is calculated at several points along the experimental curve and these values are constant, the shape of the experimental curve is correct. If the values are not consistent within each curve, a boundary condition has been violated.

The application of the laser pulse method is limited to materials which are thin (1mm-4mm) and are still representative of the material in order to satisfy heat pulse boundary conditions. The success of the flash method depends on the ability to meet the conditions developed by Parker et al.[14] and Carslaw and Jaeger[28]:

1. The radiation pulse is uniformly distributed on the surface of the sample.
2. The duration of the incident radiation pulse is negligible compared to the time required for the heat wave to travel through the sample.
3. All heat losses in the sample are as small as possible
4. Heat flow in the sample is one dimensional.
5. The heat pulse is absorbed only at the surface of the sample.
6. Sample is homogeneous and of uniform thickness.
7. Sample is initially at a uniform temperature.
8. The thermal diffusivity is constant over the temperature rise of the sample.
9. The response of the detection system is linear with temperature.
10. The signal must be well above the noise level present in the recording system.

Satisfying Boundary Conditions

Condition 1: the radiation pulse is uniformly distributed on the surface of the sample.

From the dimensions of the sample and sample holder, 85.2% of the sample is irradiated by the laser. Alignment procedures listed in the experimental procedure section of this thesis assured that the laser fired directly on the center of the sample. The surface of the ternary rare earth sulfide samples that was irradiated showed a slight blister pattern that also proved the laser alignment.

The ruby rod laser released energy in a Gausian distribution which violated this condition. This is evident when observing the pattern on thermal paper 7.6 cm away from the laser. After

firing on the thermal paper above the sample holder which is 63.5 cm from the laser, the pattern showed a uniform energy distribution. Therefore, the pulse was uniformly distributed on the sample surface.

Condition 2: the duration of the incident radiation pulse is negligible compared to the time required for the heat wave to travel through the sample.

This condition is frequently violated when the rear face temperature response curve is affected by the shape and duration of the energy pulse. This infringement is called the finite pulse time effect which several scientists have attempted to correct. Taylor and Cape[29] reported that the shape of a ruby rod laser pulse could be approximated by a square wave. Using this approximation they corrected experimental data for the finite pulse time effect to yield reasonable results. Larsen and Koyama[30] determined the pulse time correction for their diffusivity data using contour integration. Taylor and Clark[31] implemented correction curves to simplify the finite pulse time corrections. To use these curves, the pulse shape of the laser must be found. This can be accomplished by examining the temperature versus time response of an intrinsic chromel-alumel thermocouple made with 3 mil diameter wire spot welded to a .025 mm thick tantalum strip as done by Henning and Parker[32].

Heckman[33] provided a finite pulse width correction table based on the shape of the temperature versus time curve.

In this research, the specifications of the ruby rod laser stated that the pulse time was 1 ms. This pulse time was verified by measuring the temperature versus time signal of the laser by a method developed by Henning and Parker[32]. In this experiment, the average half time was 300 ms which is significantly longer than the pulse duration.

If pulse time effect corrections were needed, the experimental curve would lag the theoretical curve from about 5% to 50% rise and lead the theoretical curve from 59% to 98% rise[12,15,34]. In this experiment, corrections were not necessary as evident by examination of the normalized voltage versus normalized time of each run.

Condition 3: all heat losses in the sample are as small as possible.

Heat losses by conduction, convection, or radiation are evident by a negative slope in the thermal diffusivity curve after the maximum temperature rise has been reached. These heat losses also depress the maximum temperature. Since the experiment was performed in a vacuum, no convection heat losses were present. Conduction heat losses were eliminated by a low thermal conductivity sample holder. If radiation heat loss corrections were necessary, the experimental curve would slightly

lag the theoretical curve from about 5% to 50% rise and lead the theoretical curve from 50% to 100% rise. A short maximum would be present followed by a smooth decline[12,15,34]. The normalized voltage versus normalized temperature curve indicated that no heat losses were observed in this experiment.

If radiation heat loss corrections were necessary, they could have been corrected for by using the method of Cowan[35], Clark and Taylor[36], or Heckman[33]. Cowan determined the values of normalized voltage at different multiples of the half time. From these voltage values, thermal diffusivity values can be corrected for radiation heat losses. The Clark and Taylor[36] method is based upon the difference in nondimensionalized curves representing various heat loss. This paper indicated that the ratio of time at a higher percent temperature rise to time at a lower percent temperature rise decreases with increasing heat loss. Heckman[33] provided a heat loss correction table based on the shape of the temperature versus time curve. Heckman[33] stated that if no heat loss was observed after $5t_{1/2}$ heat loss corrections were unnecessary. The thermal diffusivity curve did not display heat losses after $5t_{1/2}$ in this experiment.

Condition 4: the heat flow in the sample is one dimensional.

The sample thicknesses ,.159 cm to .40 cm , were so thin that radial heat flow did not occur. The zirconia sample holder

had a very low thermal conductivity, .22 W/mK at 1000 °C, to minimize heat conduction out the sides of the sample that were in contact with a small lip of the sample holder such that heat flow was only one dimensional.

Condition 5: the heat pulse is absorbed only at the surface of the sample.

The penetration depth for metals is approximately 6 nm while the samples in this experiment were 2 X 10^6 nm thick, therefore only .0003% of the sample thickness absorbed the heat pulse.[37] When the heat pulse is very short, all nontransparent materials satisfy this condition due to their absorption characteristics.

Condition 6: the sample is homogeneous and of uniform thickness.

Micrographs revealed that a second phase, thought to be R_2O_2S, was present in the samples at the grain boundaries. This second phase was randomly distributed in 2% to 21.9% of the total sample. The samples are not representative of the $La_{3-x}R_xS_4$ structure in some cases, but they are homogeneous as evident in the micrographs in Appendix 3. The sample thickness was measured at several locations with a Vernier caliper which was accurate to ±.0005 cm resulting in an error of .3% for the thinnest sample. Most of the samples in this research were of uniform thickness if a slight variation in thickness was observed an average was

calculated of all measurements.

Condition 7: the sample is initially at a uniform temperature.

The average sample size was so small, 1.27 cm diameter by .2 cm thick, that there would have to be enormous temperature gradients present to cause a temperature deviation in the sample. Three tantalum radiation shields surrounded the furnace. Nine tantalum rings at half inch increments above the sample provided radiation shielding. These shields assured that no gradients were present in the furnace, thus the sample was at a initial uniform temperature.

Condition 8: the thermal diffusivity is constant over the temperature rise of the sample.

This condition was verified by observing the normalized voltage versus normalized time plot as compared to the theoretical model. The experimental curve lied on the theoretical curve, thus the thermal diffusivity values were equal at any point making this condition valid. No finite pulse or heat loss effects were present so it can be assumed that the experimental values follow the mathematical model (equation 3).

Condition 9: the response of the detection system is linear with temperature.

The spectral response curve of the InSb IR detector indicates that the response of the detector was not linear over wide temperature ranges. In this experiment, the response of the

IR detector increased from 400 °C to 800 °C where the sensitivity no longer increased. Its nonlinearity was due to the fact that the intensity of radiation given off from a body is a nonlinear function of temperature from Planck's law of black body radiation. The biggest temperature gradient observed during the thermal diffusivity experiments was about 4 °C. This gradient was so small that the detector's nonlinearity had little effect on the thermal diffusivity measurements, thus this condition was valid.

Condition 10: the signal must be well above the noise level present in the recording system.

The InSb IR detector had a signal to noise ratio of 10750. The signal to noise ratio of the thermal diffusivity curve on the oscilloscope varied from 4 to >35. Noise spikes were removed by a smoothing routine in the computer program. Other noise present was eliminated by fitting the data to a polynomial. The curves captured by the thermal diffusivity apparatus exhibited little or noise present making this condition valid.

Errors of the Flash Diffusivity Method

Measurement errors are those associated with uncertainties that exist in measured quantities in equation 4. These errors include determining the effective sample thickness and measuring the proper time at certain percentages of maximum temperature

rise. Measurement errors were reduced to <1% by using a digital data-acquisition system so only the nonmeasurement errors will be discussed. Nonmeasurement errors are associated with deviations from the boundary conditions of the mathematical model. Conditions 2 and 3 are most frequently violated in such experiments, as previously discussed these conditions have been fully met in our experimental set-up.

APPARATUS

The thermal diffusivity apparatus is capable of automated data acquisition over a temperature range of 25 to 1200 °C in a vacuum of 1 X 10^{-8} Torr. Five basic components made up the apparatus as shown in Figure 4: the vacuum chamber, heating system, pulse source, detection and amplification system, and recording and analysis assembly. The system ultimately provided the back face thermal history as a function of time and then calculated thermal diffusivity values using the known value of sample thickness. Careful attention was paid to the boundary conditions while designing the apparatus. Several authors have described their experimental set-ups to take flash diffusivity measurements[14,38,39,40].

The vacuum chamber was always kept under vacuum. An Edwards roughing pump evacuated the chamber down to .01 Torr. This roughing pump was mounted to a rubber and cork board that damped its vibration. The roughing pump was positioned five feet away from the apparatus to eliminate noise due to mechanical vibrations. An Edwards diffusion pump enabled the system to be pumped down to 1 X 10^{-8} Torr. The vacuum chamber was water cooled to ensure faster establishment of the furnace and sample temperature. This cooling also ensured that the 0-ring connecting the chamber halves would not get too hot.

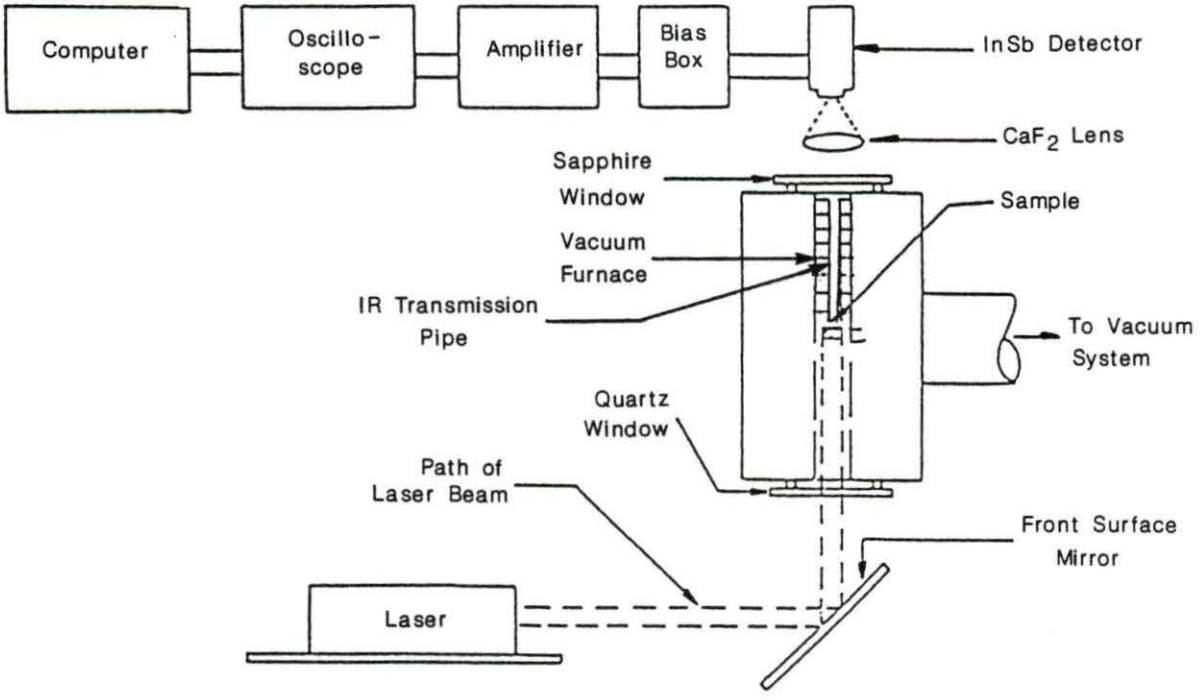

Figure 4. Thermal diffusivity apparatus

The vacuum chamber was equipped with two windows as shown in Figure 4. A quartz window at the bottom for entrance of the laser pulse, and a sapphire window at the top to transmit radiation to the infrared detector that measured the temperature transient. The quartz window was near perfect transmitting in the .29 to 2.0 micron range (ruby rod laser wavelength was .694 microns) and withstood the thermal shock of the laser. The sapphire window had excellent infrared transmitting properties in the .25 to 5.5 micron range. These windows were purchased from MDC Vacuum Products Corporation with standard flanges attached.

The sample holder centered in the furnace within the high vacuum chamber was made of zirconia insulating board type ZYFB6 manufactured by LEICO Industries. This material withstood temperatures up to 4000 °F, had exceptional strength (300 psi flexural and 230 psi compressive), very low thermal conductivity (.22 W/mK at 1100 °C), and low thermal expansion ($6X10^{-6}$ in/in at 2600 °F in air). The thermal conductivity at 700 °C of the zirconia board was 241 times less than that of boron nitride which was initially used as the sample holder. The zirconia board was moisture resistant and could be machined easily. The sample holder supported half inch diameter samples of various thicknesses. The holder was designed so that the sample would touch the zirconia around its bottom circumference to minimize

conduction heat losses. The sample and support blocked light so that the laser beam could not pass directly to the detector, because if it did the laser beam would damage the detector.

The heating system was controlled by a Love Controls 300 series universal microprocessor temperature control. A variac capable of handling 28 amps limited the current supplied to the power unit. The power unit supplied the necessary current to heat up the furnace which consisted of .031" diameter tantalum wire wrapped around a boron nitride tube. Power cables to the controller and power unit were shielded with a stainless steel mesh cable to eliminate noise in the detection system. Three tantalum radiation shields were positioned around the furnace, and nine tantalum rings at half inch increments were spot welded to the tantalum infrared transmission pipe to assure a stable furnace temperature. A platinum versus platinum-13%rhodium thermocouple was positioned in the furnace wall at the height of the sample to assure an accurate furnace temperature. The tantalum wire furnace was capable of reaching temperatures exceeding 1200 °C.

To verify the sample temperature, a thermocouple was spot welded to an armco iron sample placed inside the furnace. The temperature of the sample was compared to that of the furnace thermocouple, and the furnace temperature was always within 4 °C

of the sample temperature. The Love Controls temperature control kept the temperature within 1 °C of the set point thus the highest deviation was 5 °C.

The energy pulse was supplied to each sample by a Holobeam 600 water cooled ruby rod laser. This laser was chosen because of its high energy release (31 J) in a short pulse duration (<1ms). The laser unit consisted of a laser head (.5" in diameter by 6" in length), power supply, and water-to-air heat exchanger. The pulse wavelength of the ruby rod laser was .6943 microns. The laser was fired manually from a remote station located outside of the room in which the laser was housed. This insured the safety of the operator. The remote station also controlled the voltage to which the power supply capacitor bank was charged which determined the laser output energy. A Newport high power laser mirror reflected the ruby rod laser pulse 90 degrees onto the sample face as shown in Figure 4. This mirror had a certified damage threshold which assured survivability and maximum beam delivery in ruby laser applications.

The back face temperature rise was obtained from either a thermocouple spot welded to the sample or an indium antimonide infrared detector. Unfortunately, there were many problems encountered when using a thermocouple. Measurements were influenced by the relative rate of heat loss down the

thermocouple legs. The rate of heat loss was affected by the wire's diameter, thermal conductivity and hemispherical emittance, position relative to the sample, temperature of the hot junction, and contact conductance[12]. Errors also resulted because the energy density profile across the laser beam is nonuniform and the thermocouple monitors the temperature over a very small area. A radiation detector has the advantage of measuring an average temperature of the sample area instead of just one point.

Many of the problems associated with the thermocouple can be avoided using an optical solid state photodetector. Photovoltaic detectors produce a voltage proportional to the incident radiation. These detectors eliminate contact conductance because it is a noncontact temperature measuring device. Advantages of photodiode detectors are that they are stable, have high quantum efficiency, low thermal mass, high sensitivity, and rapid rise time.[12]

The most popular and sensitive infrared detectors from 1.0 μm to 5.5 μm are indium antimonide. A new bottom viewing InSb infrared (IR) detector purchased from Infrared Associates was used to measure the backface temperature rise. Its sapphire window assured that the sample radiation would be detected. A Melles Griot heat transmitting mirror only transmitted radiation over 700 nm to guarantee that laser light would not damage the 3

mm diameter indium antimonide chip. A pumpable dewar enabled the detector to be liquid nitrogen filled to operate at 77 K for eight hours. This provided a signal to noise ratio of 10750 and a time constant of less than 1 μs. The InSb detector performed optimally at zero voltage with the aid of a voltage offset box developed at Battelle laboratory[41]. When the background radiation shifted the operating curve, this reverse bias circuit was used to bring it back to its optimum zero voltage operating point. This offset voltage allowed the InSb IR detector to operate where maximum detectivity is achieved and the oscilloscope to be set as sensitive as possible.

The detector was placed as close as possible to the sample because of the weaker signal at greater distances as described by the inverse square law of radiation distribution. A calcium fluoride lens with a diameter of 5 cm and a focal length of 150 mm focussed the infrared radiation into the center of the detector. Calcium fluoride has excellent transmission from 150 nm to 9 microns. A darkroom black cloth curtain surrounded the infrared detector to block out atmospheric radiation. The tantalum infrared transmission pipe positioned inside the vacuum chamber between the sample and the sapphire window without touching either allowed the IR detector to focus directly on the sample.

The transient temperature versus time data was recorded on a Gould 4035 oscilloscope from the amplified IR detector signal. The voltage signal captured on the oscilloscope represented the temperature profile on the back face of the sample. The oscilloscope was externally triggered by the laser controller such that both were activated simultaneously. The computer accepted the data from the oscilloscope via an IEEE bus.

A computer program enabled the user to smooth data, select the baseline and plateau of the thermal diffusivity curve, and determine the proper degree of polynomial fit.[42] This polynomial fit to the thermal diffusivity data was an approximation of the theoretical model. The order of the polynomial was altered from 2 to 7, and the residual variance of each fit was observed. The best polynomial fit was the degree which gave the largest decrease in residual variance over the last degree. The program also calculated the coefficient of determination which measured how much of the variation in the values of the dependent variable, temperature, were attributed to changes in the independent variable, time. The thermal diffusivity was calculated at several points along the polynomial curve and an average was calculated. After these calculations, a hardcopy was attained as shown in Figure 5. The three columns of numbers on the thermal diffusivity plot represent time in seconds,

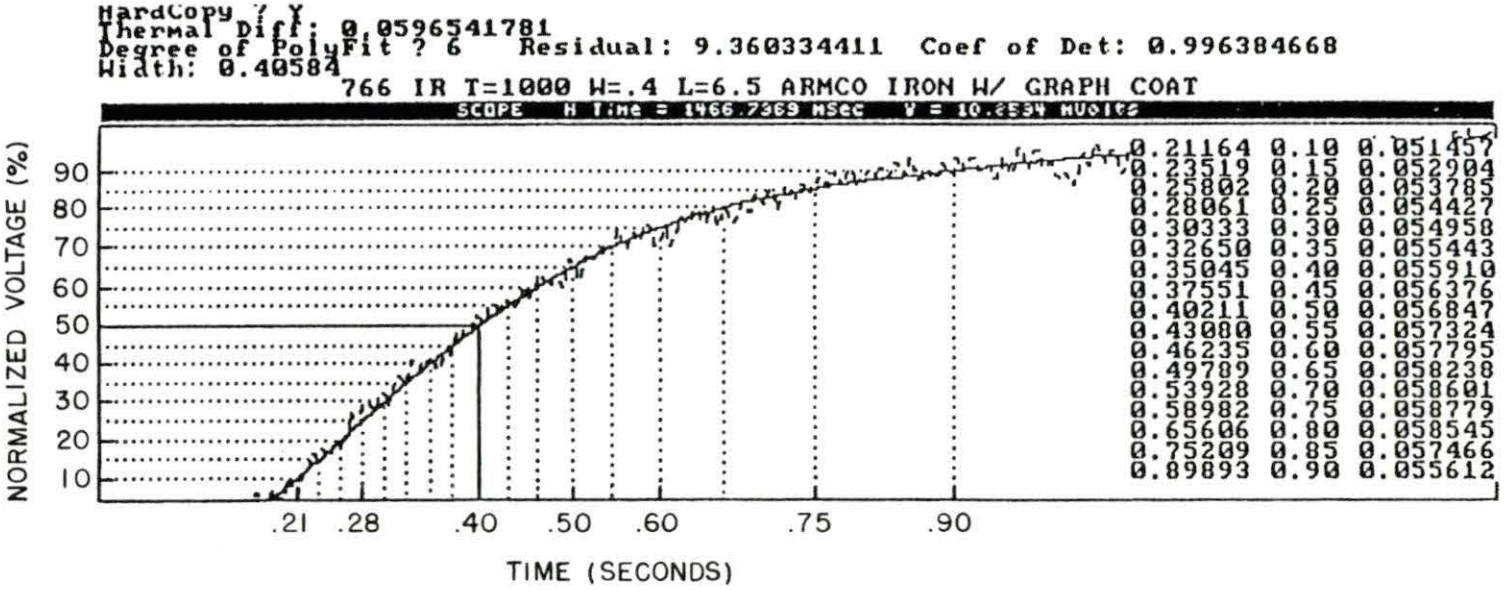

Figure 5. Thermal diffusivity curve generated by the computer program

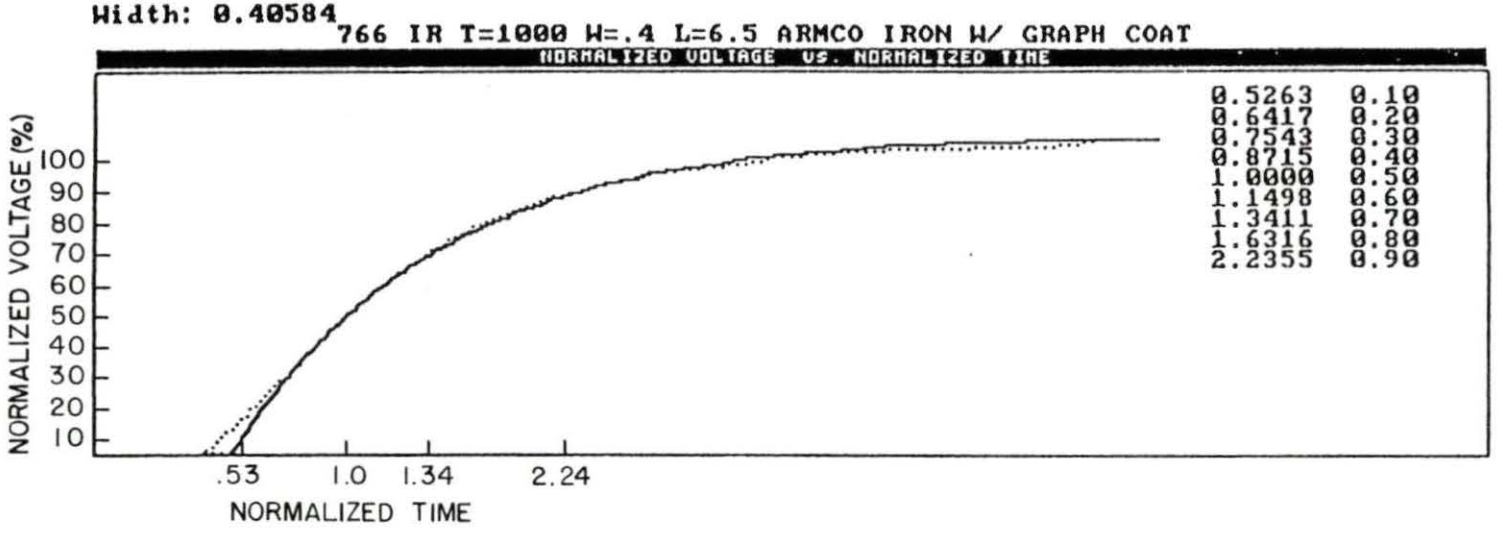

Figure 6. Experimental normalized voltage versus normalized time (dashed line) and the theoretical model (solid line)

normalized voltage, and thermal diffusivity in cm^2/s.

It is possible to compare experimental values with the theoretical model (equation 3). This was done by dividing the temperature rise by the maximum rise (normalized voltage), thus making the ordinate dimensionless. The times were divided by the half-time to make the abscissae dimensionless (normalized time).[15] This normalized voltage versus normalized time (experimental) curve was printed on the same graph as the theoretical curve as shown in Figure 6. The two columns of numbers on the the normalized voltage versus normalized time plot represent normalized time and normalized voltage respectively. The initial deviation of the experimental curve as seen in Figure 6 was due to noise from the capacitor bank discharge of the laser power supply. These curves were produced to see how well the experiment obeyed conditions 2, 3, and 8 stated in the theory section of this thesis. If these curves were not equal, finite pulse and or heat loss corrections may have been necessary.

EXPERIMENTAL PROCEDURE

Half inch diameter samples of the compositions x=.3 and x=.7 were produced for each ternary rare earth sulfide $La_{3-x}R_xS_4$ where R = Eu, Sm, and Yb. The x=.3 composition currently gives the best power factor as was shown in Figure 1. The x=.7 samples were predicted to have figure of merits comparable to SiGe alloys because it was thought that these compositions would have low thermal conductivities.

Lanthanum sulfide, the second rare earth sulfide (e.g., EuS), and lanthanum hydride were used to make the test samples. The amounts of these compounds used to make the specific compositions were calculated from the formula describing the chemical reaction that occurs in the hot press chamber[43]:

Corresponding reaction for the R=Sm and Yb ternary materials

$$(\tfrac{4}{3} - \tfrac{1}{2}x)La_2S_3 + \tfrac{1}{2}xR_2S_3 + \tfrac{1}{3}LaH_3 \Rightarrow La_{3-x}R_xS_4 + \tfrac{1}{2}H_2$$

Corresponding reaction for the Eu ternary materials

$$\tfrac{1}{3}(4-x)La_2S_3 + xEuS + \tfrac{1}{3}(1-x)LaH_3 \Rightarrow La_{3-x}Eu_xS_4 + \tfrac{1}{2}(1-x)H_2$$

For each sample produced, stoichiometric amounts of the reactants were sieved (150 mesh), weighed, mixed, and packed into a graphite sleeve inside of a glove box. Exposure to air was minimized by transporting the die from the glove box to the hot press in a helium filled plastic bag. The samples were prepared

by the pressure-assisted reaction sintering (PARS) method to assure that low porosity, crack free, low oxygen, and single phase samples were produced[43]. The PARS method produced high density pellets by the application of a double action die at high temperature for the appropriate reaction time; these samples have considerably fewer voids and concentration gradients than those produced by a cold press technique. The densities of PARS samples have reached 97% of theoretical values[43]. An induction furnace supplied a temperature of 1550 °C such that LaH_3 decomposed leaving a fine reactive powder of La metal to fill the voids between La_2S_3 particles[43]. Each sample was heated to 1550 °C at an applied pressure of 3400 psi for two hours.

The hot pressing technique allowed the possibility of lowering the thermal conductivity by phonon-grain boundary scattering. The small grain size produced by the PARS method was favorable for grain boundary scattering[7,8]. The half inch diameter pellets were long enough to obtain chemical analysis, x-ray diffraction, metallography, Seebeck coefficient, electrical resistivity, and thermal diffusivity data.

Chemical analysis was done on the top and the bottom of each pellet that was produced. The exact chemical composition of each thermal diffusivity sample was determined by examining its distance from each end of the pellet if a small concentration

gradient was present. The x-ray data were used to determine the density of samples. Metallographs taken at the top and bottom of the pellet transverse and normal to the pressing direction indicated the phases and microstructures present. Although Seebeck and electrical resistivity data already existed, these values were determined for each sample to assure the resulting figure of merit was representative of the exact sample composition.

The electrical resistivity was measured by the standard four probe dc method using rapid current reversal. The Seebeck coefficient was measured in the same apparatus by measuring the Seebeck voltage across the Pt legs of thermocouples while a temperature gradient was applied. Thermal diffusivity values were calculated using the data obtained from the diffusivity apparatus.

Before experimentation was initiated, the laser, sample, and detector were aligned with each other. First, heat sensitive paper attached to a metal block was placed above the sample holder, and the laser was fired to verify laser to sample alignment. The paper changed color showing the energy distribution of the laser. This test assured that the entire sample was being uniformly irradiated. The laser, sample, and IR detector were aligned by placing a sample with a small hole through the center in the apparatus and shining a helium neon

laser through the ruby rod and sample hole to simulate a thermal diffusivity experiment. Apertures were placed on both sides of the ruby rod to make sure the helium neon laser went through its direct center. The high power laser mirror was mounted on a goniometer head so the laser could be positioned to travel through the quartz window and the centered hole in the sample. After transmission through the sapphire window, the alignment laser was focused into the InSb detector by the calcium fluoride lens. The detector was positioned from the lens at a distance close to the focal length, 150 mm. The maximum output of the IR detector at a given temperature was found by setting the furnace at that temperature and checking the signal output with a voltmeter at different focal lengths.

After the alignment procedure was concluded, a test sample was positioned in the apparatus and the chamber was evacuated. Liquid nitrogen was poured into the detector dewar which cooled it to 77 K to provide the maximum response, because at 300 K these devices exhibit low resistances which lower the voltage output. The furnace was set to the desired temperature and the detector circuit was zero biased to correct for background radiation. To observe the detector's signal, the oscilloscope was placed on the proper voltage and time settings. Experimentation was not initiated until thermal equilibrium was

achieved at each temperature which resulted in a steady signal on the oscilloscope with little noise present. The laser was then fired at 5.0 kV to 5.5 kV releasing 1.24 J to 5.3 J of energy that produced the temperature versus time curve on the oscilloscope.

Several data points were taken at each temperature of interest above 400 °C for the samples used for calibration. Below 400 °C, excessive noise was present in the signal generated by the IR detector making it difficult to get reliable data below this temperature. Two data points were taken at 100 °C increments from 400 °C to 1000 °C for each rare earth sulfide. The thickness of each sample was corrected for thermal expansion in the thermal diffusivity computer program. The thermal diffusivity was calculated at the 50% voltage rise of each temperature (voltage) versus time curve. The thermal diffusivity values were determined by the average of two such data points at each temperature. For future reference, hardcopies of the thermal diffusivity curve with the resulting thermal diffusivity values and the normalized voltage versus normalized time were printed. The theoretical thermal diffusivity curve based on equation 3 was printed on the same plot as the normalized voltage versus normalized time experimental curve to verify some of the boundary conditions of the experiment.

The thermal conductivity values were calculated by formula 2

(k=αCd). The thermal diffusivity values were calculated as described above. The heat capacity was determined by fitting the average raw-heat content data of $La_2S_3(\alpha)$, $La_2S_3(\gamma)$, La_3S_4, and $La_{2.65}Eu_{0.35}S_4$ by a least squares method to a second order polynomial[10]. The density was calculated from the lattice parameter. The densities of the ternary rare earth sulfides at high temperatures were corrected with thermal expansion data from Goryachev and Kutsenok[44].

Using the micrographs, the grain size of each sample was determined by the Graff-Snyder intercept method[45]. Large grain size numbers represent small grain sizes. The second particle percentage was determined by a linear analysis. The root mean square (RMS) error was determined by fitting the data to a second order polynomial and computing the RMS of all point deviations from the polynomial.

The chemical composition data shown in Table 1 indicated that most of the samples were close to the sought after compositions. However, one of the samples contained more of the divalent lanthanide than the idealized $La_{2.3}R_{0.7}S_4$ composition, $La_{2.2}Eu_{0.8}S_4$. $La_{2.7}Yb_{0.2}S_4$ contained more of the trivalent lanthanide and the $La_{2.2}Yb_{0.7}S_4$ sample contained less. These differences could be due to a miscalculation, an incorrect weighing, the partial loss of a constituent metal, or an error in the chemical analysis.

Table 1. Alloy designation of the ternary rare earth sulfides

Idealized Composition	Actual Composition	Alloy Designation
$La_{2.7}Eu_{0.3}S_4$	$La_{2.71}Eu_{0.31}S_4$	$La_{2.7}Eu_{0.3}S_4$
$La_{2.3}Eu_{0.7}S_4$	$La_{2.24}Eu_{0.79}S_4$	$La_{2.2}Eu_{0.8}S_4$
$La_{2.7}Sm_{0.3}S4$	$La_{2.67}Sm_{0.31}S_4$	$La_{2.7}Sm_{0.3}S_4$
$La_{2.3}Sm_{0.7}S_4$	$La_{2.29}Sm_{0.695}S_4$	$La_{2.3}Sm_{0.7}S_4$
$La_{2.8}Yb_{0.2}S_4$	$La_{2.72}Yb_{0.16}S_4$	$La_{2.7}Yb_{0.2}S_4$
$La_{2.3}Yb_{0.7}S_4$	$La_{2.19}Yb_{0.65}S_4$	$La_{2.2}Yb_{0.7}S_4$

RESULTS AND DISCUSSION

Standard Samples

To assure the validity of results, austenitic stainless steel and graphite thermal conductivity standards were purchased from the National Bureau of Standards (NBS). Thermal diffusivity data exist for these samples as a result of round robin studies. Armco iron, a standard since the 1960s, was also used to calibrate the thermal diffusivity apparatus. The laser pulse technique was used by all of the researchers referenced. A thermal expansion correction was made for all of the samples measured in this study.

Thermal diffusivity measurements were taken on samples .25 cm and .304 cm thick for NBS austenitic stainless steel as shown in Figure 7. The thermal diffusivity values of these samples showed a low amount of scatter, 1.37% and 2.70%, as shown in Table 2. Both samples agreed with data from Maglic[46], 2.82% and 3.38% RMS error, much better than to that of Fitzer[13], 10.89% and 10.76%. Maglic used austenitic stainless steel samples of lengths .352 cm and .25 cm thick in his study. His thermal diffusivity values were corrected for thermal expansion and radiation heat loss while Fitzer did not state if corrections were made. This plus the fact that the material has a low thermal diffusivity may explain the 10.8% deviation from results of Fitzer. The thermal

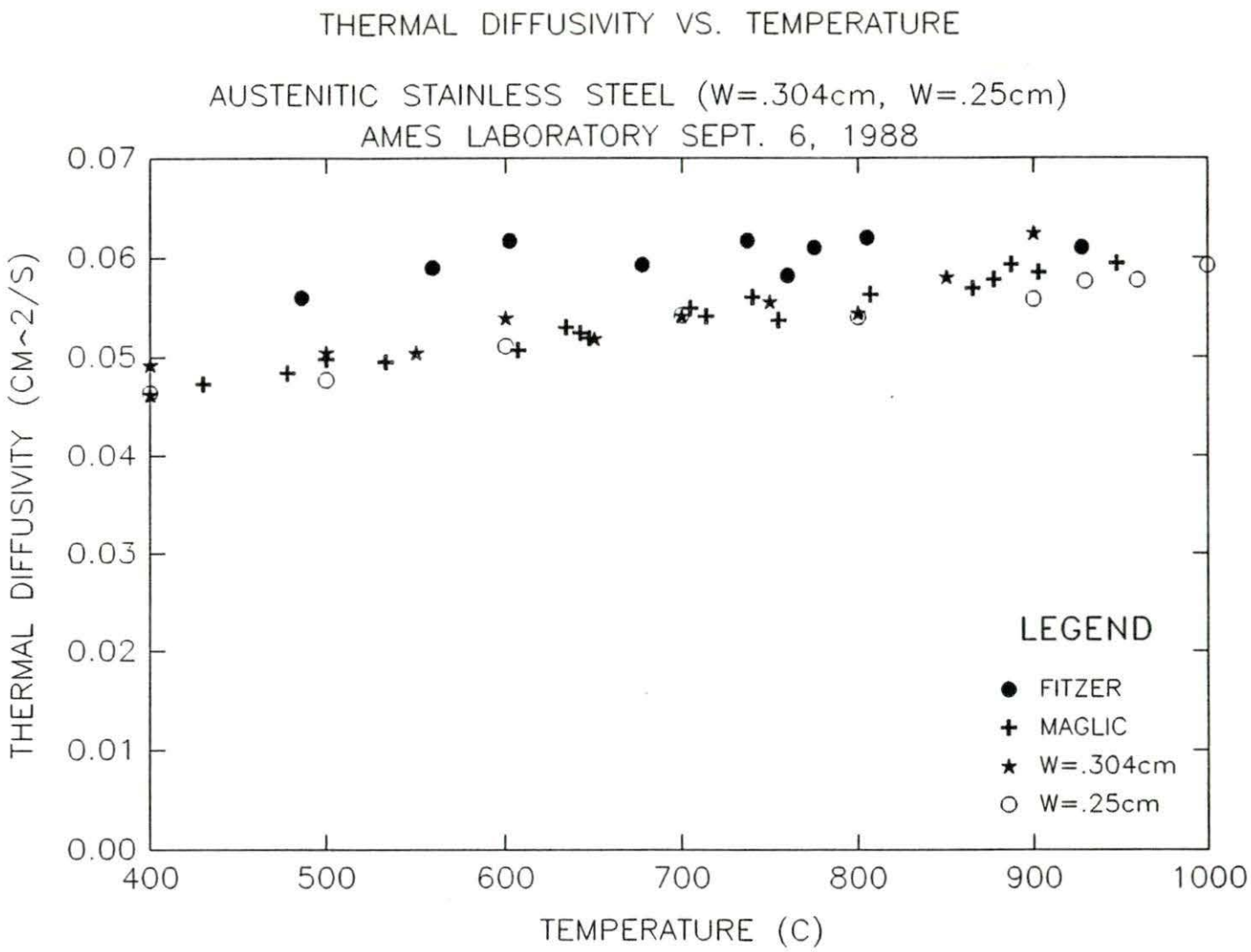

Figure 7. Thermal diffusivity versus temperature of NBS austenitic stainless steel

expansion data used were found in Fitzer[13].

A low scatter, 6.62% and 2.07%, is indicated in Table 2 for the thermal diffusivity of the .2 cm and .396 cm thick NBS graphite samples as shown in Figure 8. The .2 cm thick sample agreed well with data from Mirkovich (6.92%) and the .396 cm thick sample with Maglic (4.01%) and Taylor (7.52%).[47] Maglic used a .395 cm thick sample in his study and reported a deviation of 5% from data of Fitzer[13] above 700 °C. Of seven participants in the graphite round robin study, the variation in thermal diffusivity results of graphite was ±7%[47]. Thermal expansion data for graphite was obtained from Touloukian et al.[48]

Table 2. Error associated with the thermal diffusivity measurements of the standard samples

Sample	Thickness (cm)	Temperature Range (°C)	Standard Deviation	RMS Error (%)
Armco Iron	.283	400-740	0.0094	5.06
Armco Iron	.283	770-880	0.0048	2.59
Armco Iron	.40	400-750	0.0013	1.45
Armco Iron	.40	780-900	0.0084	1.23
Austenitic S.S.	.25	400-1000	0.0009	1.37
Austenitic S.S.	.303	400-900	0.0017	2.70
Graphite	.2	400-900	0.0147	6.62
Graphite	.396	400-990	0.0041	2.07

Figure 9 shows the thermal diffusivity of armco iron as compared to Egli[6]. The .283 cm and .4 cm thick armco iron samples had a RMS error of 5.06% and 1.45% from 400 °C

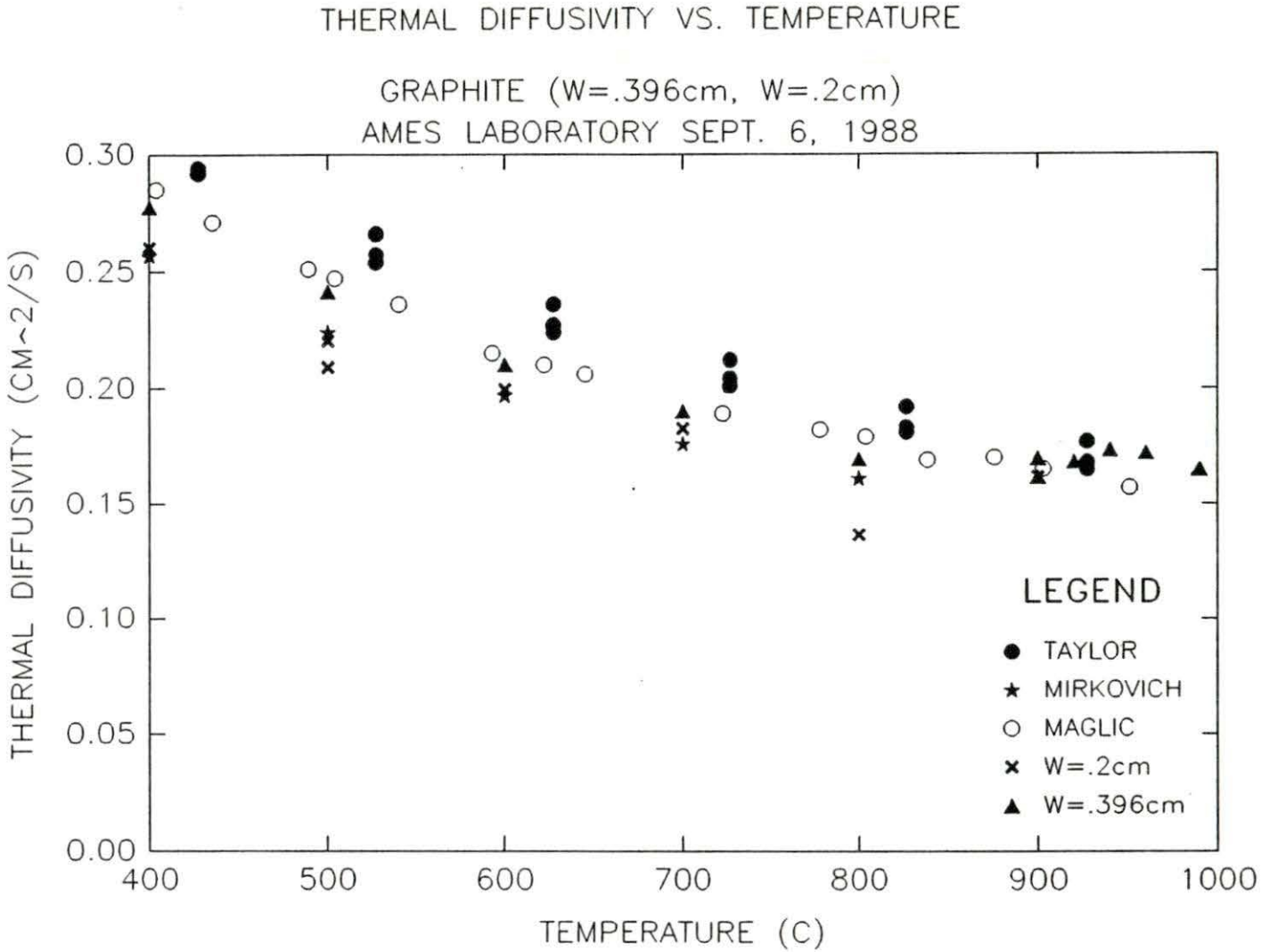

Figure 8. Thermal diffusivity versus temperature of NBS graphite

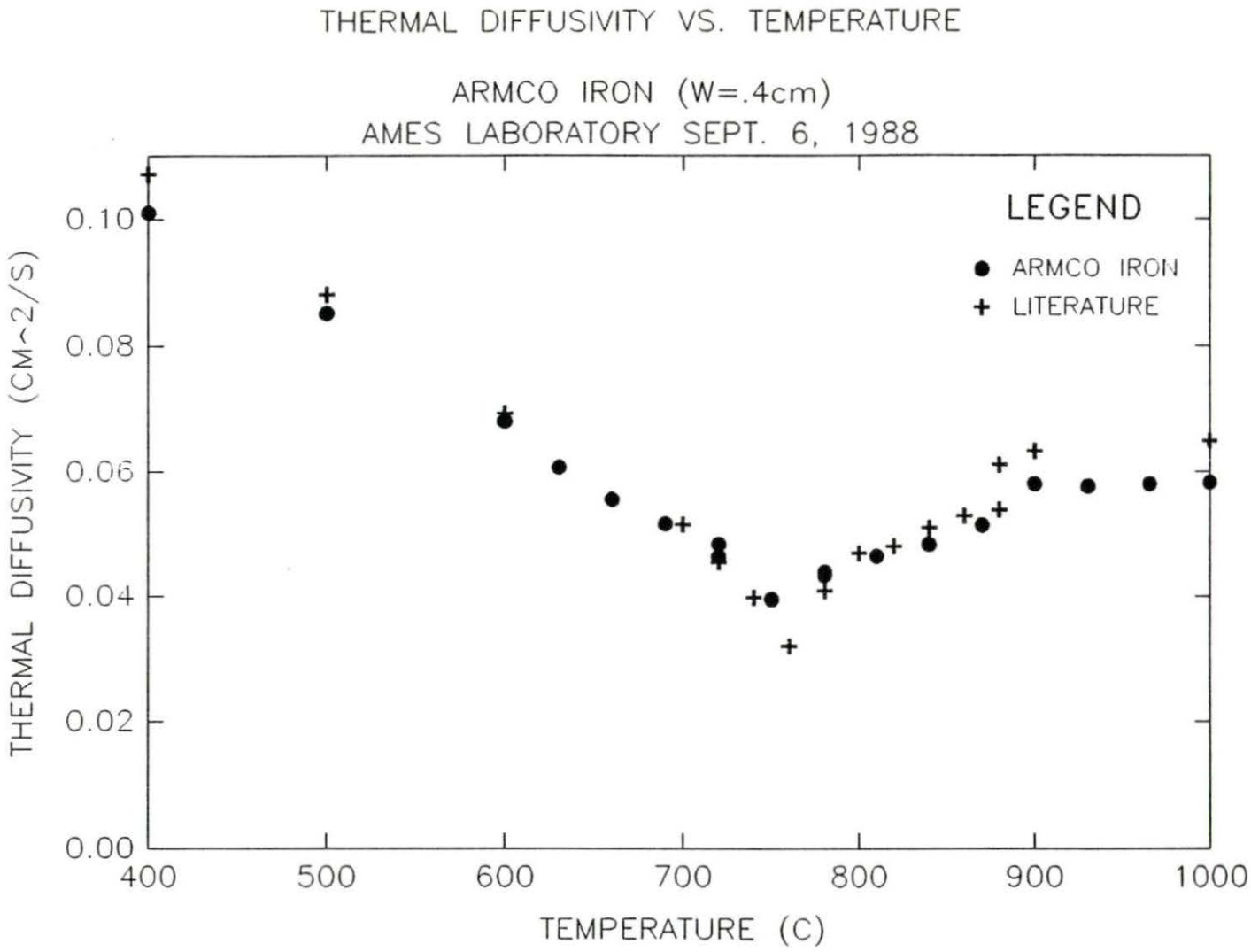

Figure 9. Thermal diffusivity versus temperature of armco iron

to 750 °C and 2.59% and 1.23% from 770 °C to 900 °C as shown in Table 2. Several investigators have reported the thermal diffusivity of armco iron[39,49,50]. For this study, the data was taken from a graph in Egli[6]. The RMS error in the data from the flash thermal diffusivity apparatus as compared to Egli ranged from 5.1% to 9.6%. The decrease in thermal diffusivity, corresponding to the abrupt increase in specific heat, near 770 °C is caused by the ferromagnetic-paramagnetic transition (769 °C is the Curie temperature), and the discountinuity at 900 °C is caused by the alpha-gamma crystalline phase transition.[6] Thermal expansion data was obtained from Smithells and Brandes[51].

Ternary Rare Earth Sulfides

The x-ray diffraction patterns showed that the ternary rare earth samples were all single phase and had the high temperature Th_3P_4-type structure. The cubic lattice parameter increased for the Eu and Sm samples as x composition increased as shown in Table 3. This was expected in the case of $La_{3-x}Eu_xS_4$ and $La_{3-x}Sm_xS_4$ because the ionic divalent Eu (.117 nm) and Sm (.119 nm) radii are larger than that of trivalent La (.1045 nm), since the ionic radius of the Yb is .100 nm the lattice constant decreased with increasing x content. This argument also explains the large lattice parameters of the $La_{3-x}Eu_xS_4$ and $La_{3-x}Sm_xS_4$ samples and the small lattice parameters of the $La_{3-x}Yb_xS_4$

samples as compared to La_3S_4[43].

Table 3. Lattice parameters for the ternary rare earth sulfides

Sample	Lattice Parameter (nm)
La_3S_4	.87280
$La_{2.7}Eu_{0.3}S_4$	.87386
$La_{2.2}Eu_{0.8}S_4$	.87460
$La_{2.7}Sm_{0.3}S_4$	.87364
$La_{2.3}Sm_{0.7}S_4$	.87423
$La_{2.7}Yb_{0.2}S_4$	.87007
$La_{2.2}Yb_{0.7}S_4$	.86696

All of the x=.7 samples had lower thermal diffusivity and thus thermal conductivity values than the x=.3 samples as shown in Figures 10 and 11. This was expected because the substitution of a divalent (Eu,Yb) or nearly divalent[3] (Sm) ion for a lanthanum ion introduces additional lattice scattering sites that lower the thermal conductivity. The x=.7 samples had more of this substitution taking place. When the electron concentration falls below a value of 2.5×10^{21}, this lattice component of the thermal conductivity is much larger than the electrical component.[52] The x=.7 samples have a more disordered lattice, thus lowering the thermal conductivity as shown in Figure 12. The lower electron concentration and small electronic contribution associated with the x=.7 samples also lowers the

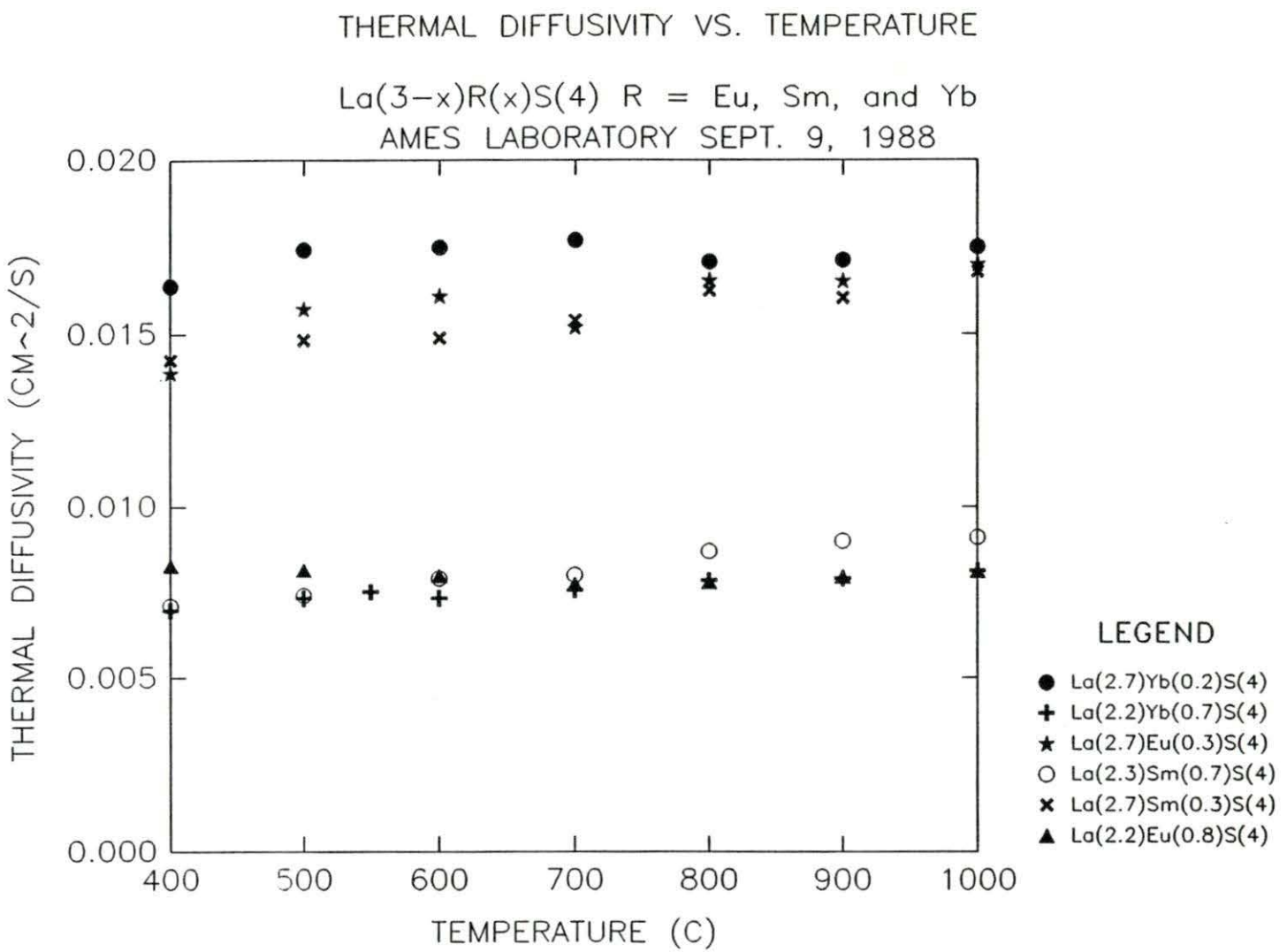

Figure 10. Thermal diffusivity versus temperature of $La_{3-x}Eu_xS_4$, $La_{3-x}Sm_xS_4$, and $La_{3-x}Yb_xS_4$ where x=.3 and .7

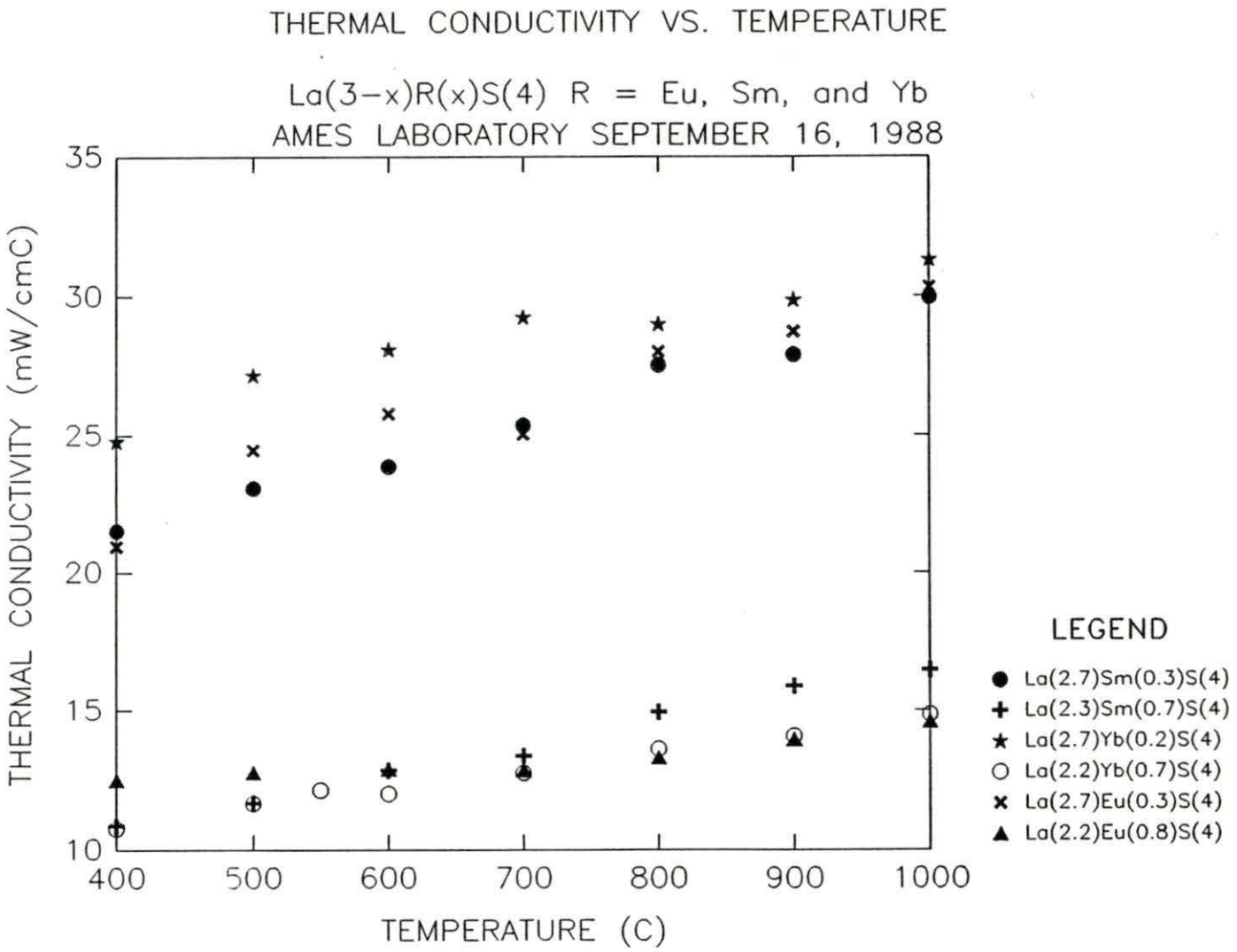

Figure 11. Thermal conductivity versus temperature of $La_{3-x}Eu_xS_4$, $La_{3-x}Sm_xS_4$, and $La_{3-x}Yb_xS_4$ where x=.3 and .7

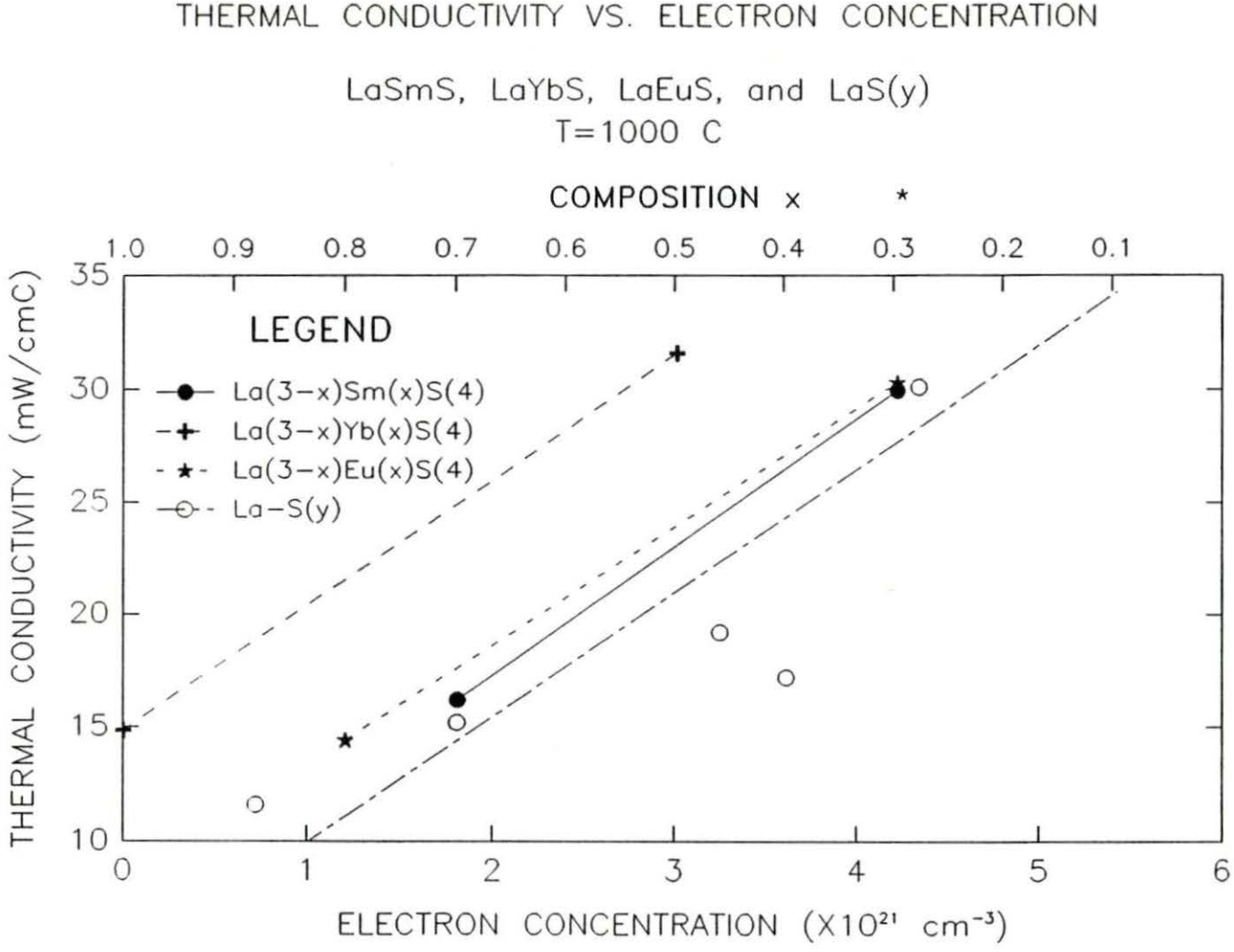

Figure 12. Thermal conductivity versus electron concentration of LaS_y, $La_{3-x}Eu_xS_4$, $La_{3-x}Sm_xS_4$, and $La_{3-x}Yb_xS_4$ where x=.3 and .7

*Top scale is not valid for the $La_{3-x}Yb_xS_4$ sample

thermal conductivity. The x=.3 samples have more electrons per unit volume which act as carriers of heat and as scatters of phonons. The former (carriers of heat) dominates the electronic contribution to the thermal conductivity[1]. The metal vacancies present in the $La_{3-x}Yb_xS_4$ samples leads to lower electron concentrations and thus their thermal conductivity values are comparable to other ternaries at low electron concentations, because the lattice component of the thermal conductivity was the dominant factor.

The thermal conductivity of the x=.3 samples decreased as the second phase percentage and grain size number increased as expected due to phonon scattering. The opposite effect was seen in the x=.7 samples due to additional lattice disorder that had the primary effect on the thermal conductivity of these samples.

In each sample, the small grain size provided more nucleation sites for the second phase as shown in Table 4. The micrographs in Appendix 3 revealed the fact that there was less of the second phase in the bulk of the samples, because less energy is required for heterogeneous nucleation at grain boundaries[53].

The second phase present in the samples is probably an oxysulfide (R_2O_2S). This compound would be expected to form before any rare earth sulfide is formed because of its large

Table 4. Microstructure qualities of the ternary rare earth sulfides

Sample	Position in Ingot	2nd Phase (%)	Grain Size (#)	Relative Grain Size
$La_{2.7}Eu_{0.3}S_4$	top	8.2	7.9	coarse
$La_{2.7}Eu_{0.3}S_4$	bottom	21.9	9.8	fairly coarse
$La_{2.2}Eu_{0.8}S_4$	top	2.7	7.0	coarse
$La_{2.2}Eu_{0.8}S_4$	bottom	2.0	4.4	coarse
$La_{2.7}Sm_{0.3}S_4$	top	2.5	4.7	coarse
$La_{2.7}Sm_{0.3}S_4$	bottom	11.1	9.0	fairly coarse
$La_{2.3}Sm_{0.7}S_4$	top	11.5	6.7	coarse
$La_{2.3}Sm_{0.7}S_4$	bottom	10.9	8.6	coarse
$La_{2.7}Yb_{0.2}S_4$	top	3.9	3.5	coarse
$La_{2.7}Yb_{0.2}S_4$	bottom	5.6	7.1	coarse
$La_{2.2}Yb_{0.7}S_4$	top	8.9	7.7	coarse
$La_{2.2}Yb_{0.7}S_4$	bottom	10.0	7.0	coarse

negative free energy of formation. Rare earth oxides have a slightly lower free energy of formation, but the ternary rare earth sulfides contain a large amount of sulfur which favors the formation of an oxysulfide.[54,55] Oxygen (2.4 at%) has been found by fast neutron activation in a $La_{2.8}Yb_{0.2}S_4$ sample with the same second phase present[56]. This oxygen could have entered the rare earth powders during their initial preparation. There was enough oxygen present in the storage glove box to turn white P_2O_5 powder brown from oxidation. It is evident by examining the second phase in the micrographs that better rare earth powder preparation and storage methods are needed to fairly assess the ternary rare earth sulfides as thermoelectric materials.

All of the samples showed a slight increase in thermal diffusivity and thermal conductivity with increasing temperature as indicated in Figures 10 and 11. At high temperatures, the number of minority carriers increases, electrons in this case, which introduce a bipolar term in the thermal conductivity. The bipolar term is directly proportional to temperature, thus the thermal conductivity increases slightly with increasing temperature. This temperature dependence was described by the least squares fit parameters shown in Tables 5 and 6. The standard deviations in Tables 5 and 6 indicated the deviation for any one point at a given temperature.

The spread in error of the thermal diffusivity and the thermal conductivity of the ternary rare earth sulfides was 1.24% to 3.5% and .78% to 3.43% respectively as indicated in Tables 5 and 6. These values are listed in Appendix 2. The low scatter was due to the precision of the flash diffusivity apparatus.

A figure of merit of .52 was found for the best ternary rare earth sulfide $La_{2.2}Eu_{0.8}S_4$ as shown in Table 7. This value is low compared to the figure of merit of SiGe alloys (.7-.8)[4] currently being used in RTGs. The $La_{2.2}Eu_{0.8}S_4$ sample had a higher figure of merit (.52) than $LaS_{1.48}$ (.5), the best

Table 5. Least squares fit parameters of the thermal diffusivity of the ternary rare earth sulfides

Sample	$\alpha = A + BT$ (cm^2/s) A(10^{-3})	B(10^{-5})	Standard Deviation	RMS (%)	Temperature Range (°C)
$La_{2.7}Eu_{0.3}S_4$	13.0121	0.406428	0.000631	3.50	400-1000
$La_{2.2}Eu_{0.8}S_4$	8.2645	-0.037737	0.000195	1.98	400-1000
$La_{2.7}Sm_{0.3}S_4$	12.6504	0.406069	0.000233	1.25	400-1000
$La_{2.3}Sm_{0.7}S_4$	5.6714	0.357141	0.000143	1.43	400-1000
$La_{2.7}Yb_{0.2}S_4$	16.6505	0.084629	0.000436	2.15	400-1000
$La_{2.2}Yb_{0.7}S_4$	6.3743	0.175517	0.000105	1.24	400-1000

Table 6. Least squares fit parameters of the thermal conductivity of the ternary rare earth sulfides

Sample	$\alpha = A + BT$ (mW/cm°C) A	B(10^{-2})	Standard Deviation	RMS (%)	Temperature Range (°C)
$La_{2.7}Eu_{0.3}S_4$	16.40338	1.412154	1.080186	3.43	400-1000
$La_{2.2}Eu_{0.8}S_4$	10.88915	0.317949	0.299983	2.27	400-1000
$La_{2.7}Sm_{0.3}S_4$	15.96012	1.377961	0.401379	1.28	400-1000
$La_{2.3}Sm_{0.7}S_4$	6.79047	0.989591	0.232648	2.14	400-1000
$La_{2.7}Yb_{0.2}S_4$	22.25375	0.930443	0.908705	2.31	400-1000
$La_{2.2}Yb_{0.7}S_4$	8.29272	0.651383	0.167149	0.78	400-1000

lanthanum sulfide as reported by Wood[5]. All the x=.7 samples exhibited higher figure of merits due to their low thermal conductivities. The $La_{2.2}Eu_{0.8}S_4$ sample had the least second phase present and thus the highest figure of merit of the x=.7 samples. Nakahara *et al.*[3] and Cook[4] reported that the second phase ,an oxysulfide, increases the Seebeck coefficient and

electrical resistivity thus decreasing the power factor. These second phase particles provided additional scattering sites which favorably lower the thermal conductivity, but raise the electrical resistivity considerably thus lowering the figure of merit. Since $La_{2.2}Eu_{0.8}S_4$ with the second phase present exhibited a higher figure of merit than $LaS_{1.48}$, the ternary rare earth sulfides look promising as thermoelectric materials. Energy dispersive x-ray spectroscopy on a scanning electron microscope should be performed on the second phase particles to identify the exact compound present.

Table 7. Experimental results at 1000 °C

Alloy Designation	Seebeck Coeff. (μV/°C)	Electrical Resist. (mΩcm)	Thermal Cond. (mW/cm°C)	Figure of Merit (X 1000 °C)
$La_{2.7}Eu_{0.3}S_4$	-120.1	1.4	30.31	.34
$La_{2.2}Eu_{0.8}S_4$	-219.1	6.34	14.426	.525
$La_{2.7}Sm_{0.3}S_4$	-108.1	1.2	29.961	.325
$La_{2.3}Sm_{0.7}S_4$	-149.8	3.4	16.20	.407
$La_{2.7}Yb_{0.2}S_4$	-101.8	1.1	31.597	.298
$La_{2.2}Yb_{0.7}S_4$	-177.3	5.6	14.845	.378

SUMMARY

The thermal diffusivity of armco iron, austenitic stainless steel, and graphite standards was determined from 400 °C to 1000 °C using the flash diffusivity apparatus. These data were compared to that of other experimenters to check the validity of results. The highest error associated with these comparisons was 10%.

The ternary rare earth sulfides $La_{2.7}Eu_{0.3}S_4$, $La_{2.2}Eu_{0.8}S_4$, $La_{2.7}Sm_{0.3}S_4$, $La_{2.3}Sm_{0.7}S_4$, $La_{2.7}Yb_{0.2}S_4$, and $La_{2.2}Yb_{0.7}S_4$ were prepared by the PARS method. These samples were all single phase and had the high temperature Th_3P_4 structure. The thermal diffusivity of these rare earth sulfides was measured over the temperature range 400 °C to 1000 °C. The thermal conductivity of these samples was calculated from the measured thermal diffusivity data, published heat capacity data, and measured density data from x-ray diffraction patterns. All of the samples showed a slight increase in thermal conductivity with increasing temperature. All of the x=.3 samples exhibited a higher thermal conductivity than the x=.7 samples with $La_{2.7}Yb_{0.2}S_4$ having the highest thermal conductivity (31.6 mW/cm°C) and $La_{2.2}Eu_{0.8}S_4$ the lowest (14.4 mW/cm°C).

The figure of merit at 1000 °C was calculated for each rare earth sulfide using measured thermal conductivity, Seebeck coefficient, and electrical resistivity data. $La_{2.2}Eu_{0.8}S_4$ had

the highest figure of merit at 1000 °C of .525 which is significantly lower than the figure of merit of SiGe alloys, .7 to .8, currently being used in RTGs. The presence of an oxysulfide at the grain boundaries degraded the high temperature thermoelectric performance of these samples. The $La_{2.2}Eu_{0.8}S_4$, even with this second phase present, exhibited a higher figure of merit (.525) than $LaS_{1.48}$ (.5). The ternary rare earth sulfides should have figures of merit that exceed .525, because the second phase present in the samples degraded their thermoelectric properties. These materials could have figure of merit values greater than SiGe alloys (.7-.8), but better sample preparation and storage methods are needed to fairly assess the ternary rare earth sulfides as thermoelectric materials.

ACKNOWLEDGEMENTS

The author wishes to thank Dr. Karl A. Gschneidner Jr. for his technical suggestions and help editing this thesis. The author is indebted to Jeff Funke, Nile Beymer, and Bruce Cook for hot pressing samples. The author wishes to acknowledge Bruce Cook for measuring the Seebeck coefficient and electrical resistivity of the samples and his suggestions throughout this research project. The author thanks Bernard Beaudry for his assistance during this experimentation. The author would also like to acknowledge Eric Knight and Jim Lavoy for their computer programming assistance. This work was performed at Ames Laboratory under contract No. W-7405-eng-82 with the U. S. Department of Energy. The United States government has assigned the DOE Report number IS-T 1391 to this thesis.

BIBLIOGRAPHY

1. Rowe, D. M.; Bhandari, C. M. Modern Thermoelectrics; Rinehart and Winston Ltd.: Eastbourne, East Sussex, 1983.

2. Beaudry, B. J. Ames Laboratory, Iowa State University, personal communication, 1987.

3. Nakahara, J. F.; Takeshita, T.; Tschetter, M. J.; Beaudry, B. J.; Gschneidner, K. A., Jr. J. Appl. Phys. 1988, 63, 2331-2336.

4. Cook, B. Ames Laboratory, Iowa State University, personal communication, 1988.

5. Wood, C.; Lockwood, A.; Parker, J.; Zoltan, A.; Zoltan, D.; Danielson, L.; Raag, V. J. Appl. Phys. 1985, 58, 1542-1547.

6. Egli, Paul H. Thermoelectricity; John Wiley and Sons: New York, New York, 1960.

7. Bhandari, C. M.; Rowe, D. M. J. Phys. C:Solid State Phys. 1987, 2, 1787-1794.

8. Vandersande, J. W.; Wood, C.; Zoltan, A.; Whittenberger, D. 19th Int. Thermal Conductivity Conf., Cookeville, TN, 1985; to be published.

9. Rowe, D. M. Applied Energy 1986, 24, 139-162.

10. Amano, T.; Beaudry, B. J.; Gschneidner, K. A. Jr. J. Appl. Phys. 1986, 59, 3437-3440.

11. Spedding, F. H.; Henderson, J. J. Chem. Phys. 1971, 54, 2476.

12. Maglic, K. D.; Cezairliyan, A.; Peletsky, V. E. Compendium of Thermophysical Property Measurement Methods; Plenum: New York, 1984; Vol. 1, p 299-336.

13. Fitzer, E. "Thermophysical Properties of Solid Materials Project Selection 2 Cooperate Measurements on Heat Transport Phenomena of Solid Materials at High Temperature"; AGARD Report No. 606, 1973.

14. Parker, W. J.; Jenkins, R. J.; Butler C. P.; Abbott G. L. J. Appl. Phys. 1961, 32, 1679-1684.

15. Taylor, R. E. High Temp. High Pres. 1979, 11, 43-58.

16. Fang, Z.; Taylor, R. High Temp. High Pres. 1987, 19, 29-36.

17. Schriempf, J. T. "A Laser-Flash Technique for Determining Thermal Diffusivity of Liquid Metals at Elevated Temperatures," Report of NRL Progress, 1972, pp 9-17.

18. Ohta, H.; Waseda, Y. High Temp. Materials and Processes 1986, 7, 179-184.

19. Amazouz, M.; Christian, M.; Degiovanni, A. High Temp. High Pres. 1987, 19, 37-41.

20. Gilchrist, K. E. "Measurement of Thermal Conductivity of Ultrathin Single or Double Layer Samples," Proc. European Conf. Thermophys. Properties of Solids at High Temps., Baden-Baden, 1968.

21. Taylor, R. E.; Groot, H.; Donaldson, A. B. "Thermal Diffusivity of HNS High Explosives," Thermal Conductivity; Plenum: New York, 1983; Vol. 16.

22. Lee, H. J.; Taylor, R. E. J. Heat Transfer 1978, 100, 720-724.

23. Lee, H. J.; Taylor, R. E. Carbon 1975, 13, 521-527.

24. Larson, K. B.; Koyama, K. J. Appl. Phys. 1968, 39, 4408-4416.

25. Lee, H. J.; Taylor, R. E. Thermal Conductivity; Plenum: New York, 1976; Vol. 14.

26. Taylor, R. E.; Lee, H. J. "Determination of Thermophysical Properties of Layered Composites by Flash Method," NTIS Report PB239-114, 1974.

27. James, H. M. High Temp. High Pres. 1985, 17, 481-496.

28. Carslaw, H. S.; Jaeger, J. C. Conduction of Heat in Solids, 2nd ed.; Oxford University Press: New York, New York, 1959.

29. Taylor, R. E.; Cape, J. A. Appl. Phys. Lett. 1964, 5, 212-213.

30. Larson, K. B.; Koyama, K. J. Appl. Phys. 1967, 38, 465-474.

31. Taylor, R. E.; Clark, L. M. III High Temp. High Pres. 1974, 6, 65-72.

32. Henning, R. C.; Parker, R. J. Heat Transfer 1967, 89, 146-154.

33. Heckman, R. C. J. Appl. Phys. 1973, 44, 1455-1460.

34. Taylor, R. E. Rev. Int. Hautes Temp. et Refract. 1975, 12, 141-145.

35. Cowan, R. D. J. Appl. Phys. 1963, 34, 926-927.

36. Clark, L. M. III; Taylor, R. E. J. Appl. Phys. 1975, 46, 714.

37. Hecht, E.; Zajac, A. Optics, 3rd ed.; Addison-Wesley: Philippines, 1976; pp 84-88.

38. Taylor, R. Phys. E. Sci. Instrum. 1980, 13, 1193-1199.

39. Rudkin, R. L.; Jenkins, R. J.; Parker, W. J. Rev. Sci. Instrum. 1962, 33, 21-24.

40. Wood, C.; Zoltan, A. Rev. Sci. Instrum. 1984, 55, 235-237.

41. Ogden, J. S. Battelle Laboratory, Columbus Division, personal communication, 1987.

42. Hood, W. G. Byte 1987, 12, 155-160.

43. Takeshita, T.; Gschneidner, K. A., Jr.; Beaudry, B. J. J. Appl. Phys. 1985, 57, 4633-4635.

44. Goryachev, Y. M.; Kutsenok, T. G. High Temp. High Pres. 1972, 4, 663-669.

45. Kehl, G. L. Principles of Metallographic Laboratory Practice, 3rd ed.; Mc Graw Hill: New York, 1949; pp 292-293.

46. Maglic, K. D.; Perovic, N.; Zivotic, Z. High Temp. High Pres. 1980, 12, 555-560.

47. Hust, G. H. A Fine-Grained, Isotropic Graphite for Use as NBS Thermophysical Property RM's from 5 to 2500 K. U.S. Department of Commerce/National Bureau of Standards. U.S. Government Printing Office: Washington, DC, 1984; NBS Special Publication 260-89.

48. Touloukian, Y. S.; Kirby, R. K.; Taylor, R. E.; Lee T. Y. R. Thermophysical Properties of Matter; Plenum: New York, 1977; Vol. 13, p. 75.

49. Sidles, P. H.; Danielson, G. C. In Thermoelectricity; Egli, P. H., Ed.; John Wiley and Sons Inc.: New York, 1960; pp 270-288.

50. Touloukian, Y. S.; Powell, R. W.; Ho, C. Y.; Nicolaou, M. C. Thermophysical Properties of Matter; Plenum: New York, 1973; Vol. 10.

51. Smithells, C. J.; Brandes, E. A. Metals Reference Book, 5th ed.; Butterworths: Boston, 1976.

52. Gschneidner, K. A. Jr.; Nakahara, J. N.; Beaudry, B. J.; Takeshita, T. In Materials Research Society Symposia Proceedings; Emin, D.; Aselage, T. L.; Wood, C., Ed.; Publishers Choice Book Mfg. Co.: Mars, Pennsylvania, 1987; Vol. 97, pp 359-370.

53. Verhoeven, J. D. Fundamentals of Physical Metallurgy; John Wiley and Sons: New York, 1975; pp 217-230.

54. Gschneidner, K. A., Jr.; Kippenhan, N.; Mc Masters, D. O. Thermochemistry of the Rare Earths; Rare Earth Information Center, Iowa State University.

55. Vaughan, C. M.; White, W. B. In Materials Research Society Symposia Proceedings; Emin, D.; Aselage, T. L.; Wood, C., Ed.; Publishers Choice Book Mfg. Co.: Mars, Pennsylvania, 1987; Vol. 97, pp 397-402.

56. Nakahara, J. F. Ames Laboratory, Iowa State University, personal communication, 1987.

APPENDIX 1: DERIVATION OF THE THERMAL DIFFUSIVITY AT 1/2 MAXIMUM TEMPERATURE RISE

The following equation was developed by Carslaw and Jaeger to describe the resulting temperature-time curve of the back face from a burst of radiant energy..

$$(3) \qquad V = \frac{T_m}{T_{L,t}} = 1 + 2\Sigma(-1)^n \exp\left(- \frac{n^2\pi^2\alpha t}{L^2}\right)$$

Where V = Fraction of the maximum temperature rise
T_m = Maximum temperature (°C)
$T_{L,t}$ = Temperature at some length, l, after some time, t, (°C)
n = Number of terms
α = Thermal Diffusivity (cm^2/s)
t = Time (s)
L = Thickness of sample (cm)

To find the thermal diffusivity at 1/2 the maximum temperature rise, take the first term of equation 3 and let V=.5.

$$.5 = 1 + 2\left(- \exp - \frac{\pi^2\alpha t}{L^2}\right)$$

$$-.5 = 2\left(- \exp - \frac{\pi^2\alpha t}{L^2}\right)$$

$$\frac{.5}{2} = \exp - \frac{\pi^2\alpha t}{L^2}$$

$$\ln \frac{.5}{2} = - \frac{\pi^2\alpha t}{L^2}$$

$$1.38 = \frac{\pi^2\alpha t}{L^2}$$

$$(4) \qquad \alpha_{1/2} = \frac{1.38\ L^2}{\pi^2\ t_{1/2}}$$

where $\alpha_{1/2}$ = Thermal diffusivity at 1/2 maximum temperature (cm^2/s)
L = Sample thickness (cm)
$t_{1/2}$ = Time to reach 1/2 maximum temperature (s)

APPENDIX 2: THERMAL DIFFUSIVITY AND THERMAL CONDUCTIVITY RESULTS OF THE TERNARY RARE EARTH SULFIDES

THERMAL CONDUCTIVITY CALCULATION FOR LA(2.7)Eu(0.3)S(4) AT WT = 548.8715 g/mole

B = 118.359 C = .0259298 ROOM DENSITY = 5.4652 g/cm^3

TEMPERATURE (C)	THERMAL DIFF (cm^2/s)	SPECIFIC HEAT (J/gC)	DENSITY (g/cm^3)	THERMAL COND (mW/cmC)
400	.01389	.2792284	5.4038517	20.95874
500	.01573	.2886768	5.3877332	24.465083
600	.0161	.2981252	5.3716787	25.78306
700	.0152	.3075736	5.3556879	25.038478
800	.01655	.317022	5.3397605	28.01619
900	.01653	.3264704	5.3238963	28.73070
1000	.017	.3359188	5.3080948	30.31251

THERMAL CONDUCTIVITY CALCULATION FOR La(2.3)Eu(0.7)S(4) AT WT = 554.0935 g/mole

B = 118.359 C = .0259298 ROOM DENSITY = 5.5004 g/cm^3

TEMPERATURE (C)	THERMAL DIFF (cm^2/s)	SPECIFIC HEAT (J/gC)	DENSITY (g/cm^3)	THERMAL COND (mW/cmC)
400	.008228	.2765968	5.4386566	12.37750
500	.0081395	.2859562	5.4224342	12.62093
600	.0079765	.2953156	5.4062763	12.734941
700	.007734	.3046749	5.3901826	12.701188
800	.007793	.3140343	5.3741526	13.15199
900	.007959	.3233936	5.3581862	13.79138
1000	.008115	.332753	5.3422829	14.425716

THERMAL CONDUCTIVITY CALCULATION FOR LA(2.7)Sm(0.3)S(4) AT WT = 548.4035 g/mole

B = 118.359 C = .0259298 ROOM DENSITY = 5.4647 g/cm^3

TEMPERATURE (C)	THERMAL DIFF (cm^2/s)	SPECIFIC HEAT (J/gC)	DENSITY (g/cm^3)	THERMAL COND (mW/cmC)
400	.01426	.2794667	5.4033573	21.53343
500	.01483	.2889232	5.3872403	23.08287
600	.01489	.2983796	5.3711872	23.86350
700	.01539	.3078361	5.3551979	25.37077
800	.01625	.3172926	5.339272	27.52930
900	.01604	.326749	5.3234092	27.90027
1000	.01679	.3362055	5.3076091	29.96087

THERMAL CONDUCTIVITY CALCULATION FOR LA(2.3)Sm(0.7)S(4) AT WT = 553.0015 g/mole
B = 118.359 C = .0259298 ROOM DENSITY = 5.498 g/cm^3

TEMPERATURE (C)	THERMAL DIFF (cm^2/s)	SPECIFIC HEAT (J/gC)	DENSITY (g/cm^3)	THERMAL COND (mW/cmC)
400	.0071	.277143	5.4362835	10.69705
500	.0074	.2865209	5.4200683	11.49192
600	.0079	.2958987	5.4039174	12.63219
700	.008	.3052766	5.3878307	13.15822
800	.0087	.3146544	5.3718077	14.70528
900	.009	.3240322	5.3558482	15.61920
1000	.0091	.3334101	5.3399519	16.20158

THERMAL CONDUCTIVITY CALCULATION FOR LA(2.8)YB(02.)S(4) AT WT = 551.782 g/mole
B = 118.359 C = .0259298 ROOM DENSITY = 5.5633 g/cm^3

TEMPERATURE (C)	THERMAL DIFF (cm^2/s)	SPECIFIC HEAT (J/gC)	DENSITY (g/cm^3)	THERMAL COND (mW/cmC)
400	.01638	.2777555	5.5008505	25.02686
500	.01742	.2871541	5.4844427	27.43441
600	.01749	.2965527	5.4681	28.36142
700	.0177	.3059512	5.4518222	29.52345
800	.01708	.3153498	5.4356089	29.27713
900	.01713	.3247484	5.4194599	30.14812
1000	.0175	.3341469	5.4033747	31.59662

THERMAL CONDUCTIVITY CALCULATION FOR LA(2.3)YB(0.7)S(4) AT WT = 568.8495 g/mole
B = 118.359 C = .0259298 ROOM DENSITY = 5.8005 g/cm^3

TEMPERATURE (C)	THERMAL DIFF (cm^2/s)	SPECIFIC HEAT (J/gC)	DENSITY (g/cm^3)	THERMAL COND (mW/cmC)
400	.00697	.2694219	5.7353879	10.77031
500	.00732	.2785385	5.7182805	11.65901
550	.00751	.2830968	5.7097523	12.13925
600	.00732	.287655	5.701241	12.00473
700	.00756	.2967716	5.6842692	12.75318
800	.00785	.3058882	5.6673646	13.60860
900	.0079	.3150048	5.650527	14.06154
1000	.00813	.3241214	5.6337561	14.84554

APPENDIX 3: METALLOGRAPHS OF THE TERNARY RARE EARTH SULFIDES

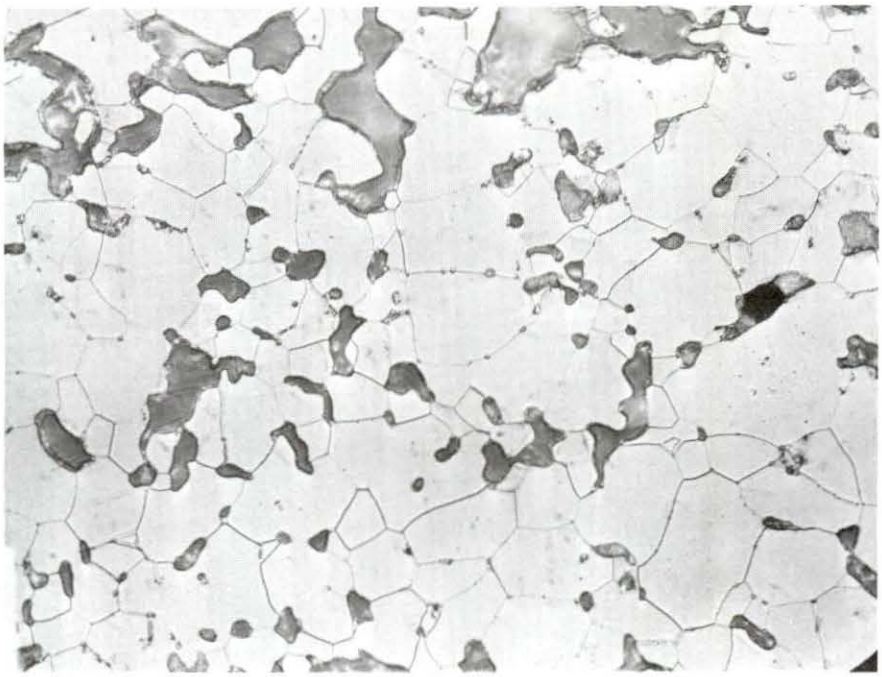

Metallograph 1: $La_{2.7}Eu_{0.3}S_4$ top of ingot horizontal slice 500X.

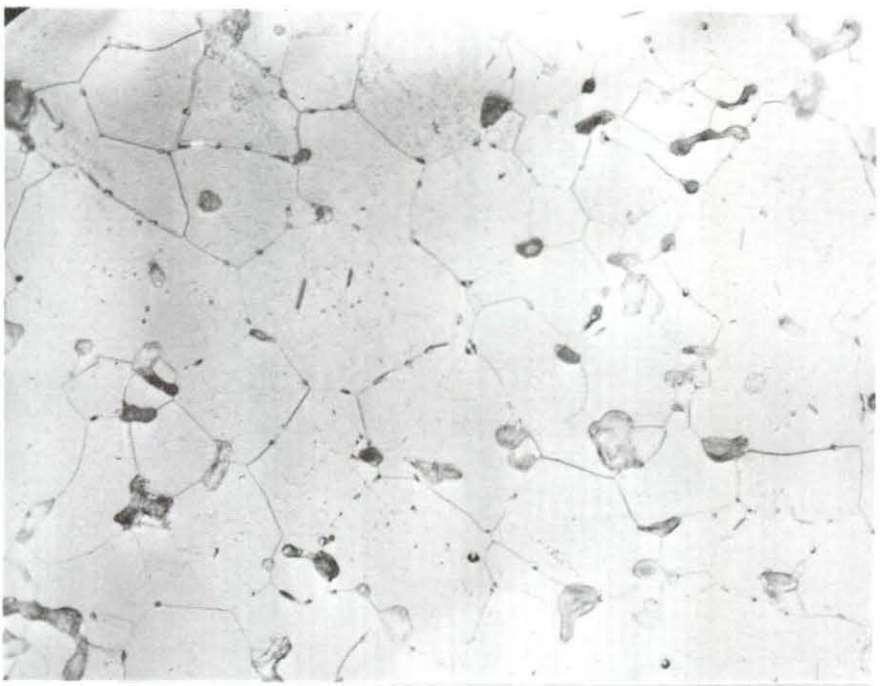

Metallograph 2: $La_{2.7}Eu_{0.3}S_4$ top of ingot vertical slice 500X.

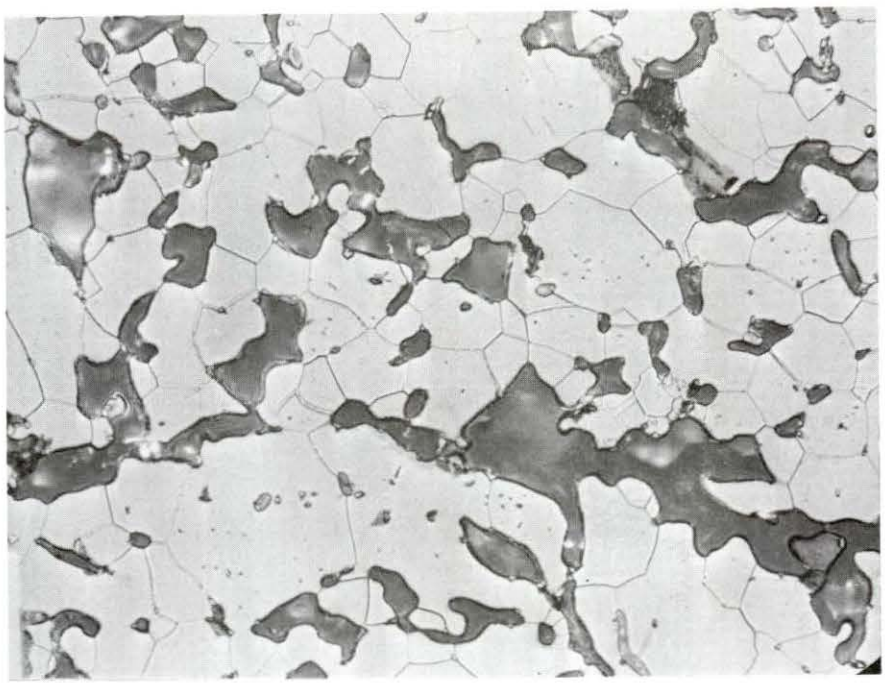

Metallograph 3: $La_{2.7}Eu_{0.3}S_4$ bottom of ingot horizontal slice 500X.

Metallograph 4: $La_{2.7}Eu_{0.3}S_4$ bottom of ingot vertical slice 500X.

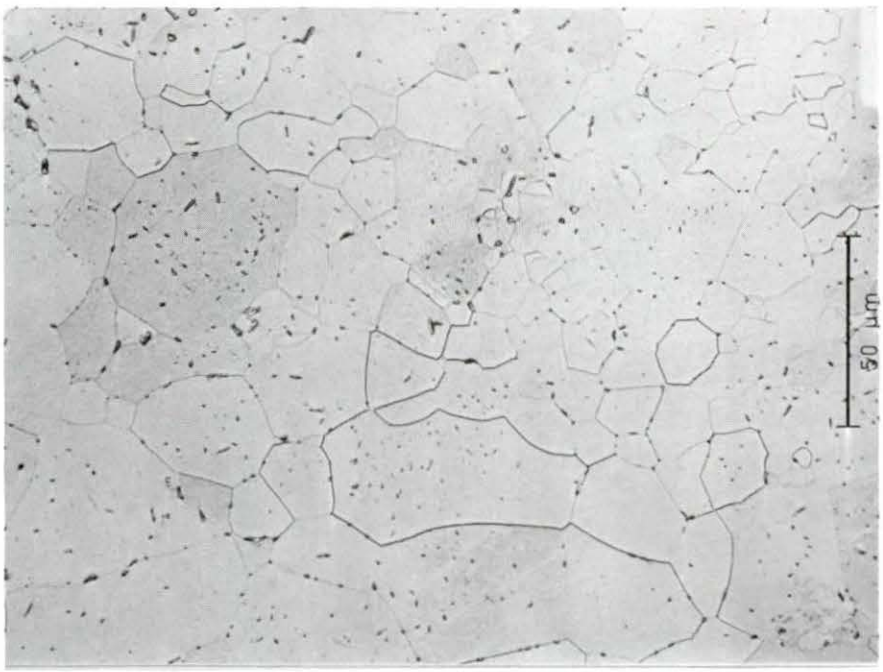

Metallograph 5: $La_{2.3}Eu_{0.7}S_4$ top of ingot horizontal slice 500X.

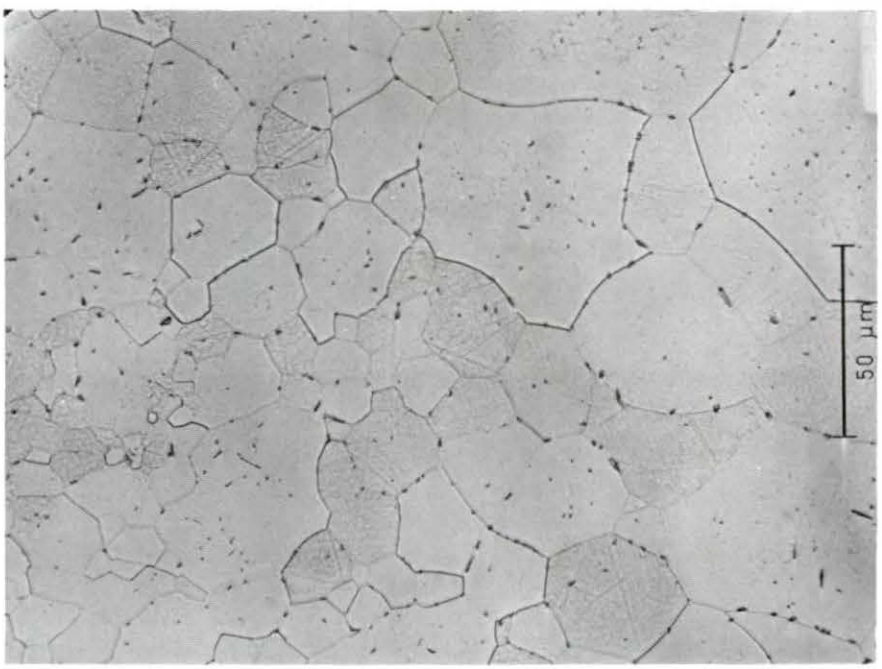

Metallograph 6: $La_{2.3}Eu_{0.7}S_4$ top of ingot vertical slice 500X.

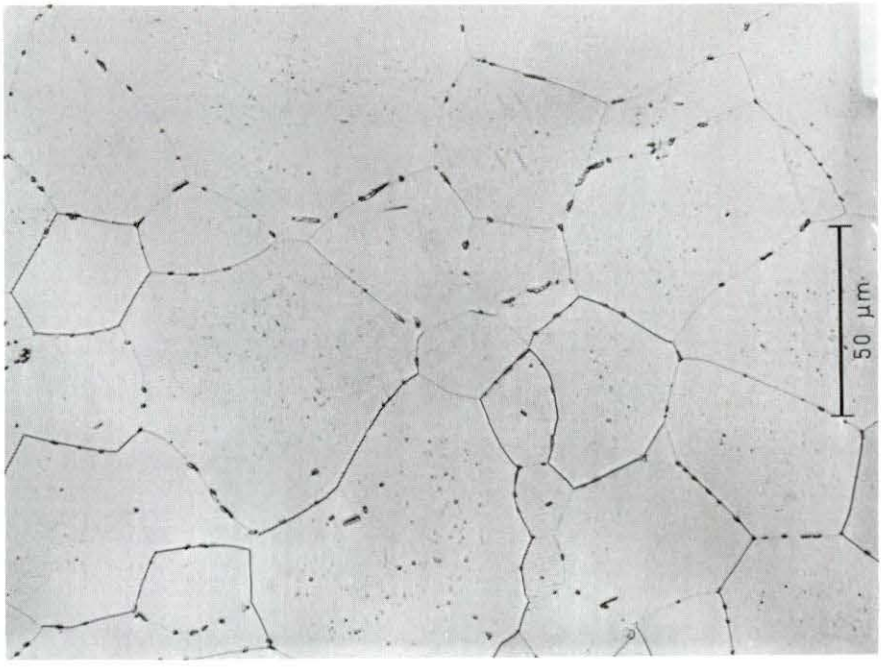

Metallograph 7: $La_{2.3}Eu_{0.7}S_4$ bottom of ingot horizontal slice 500X.

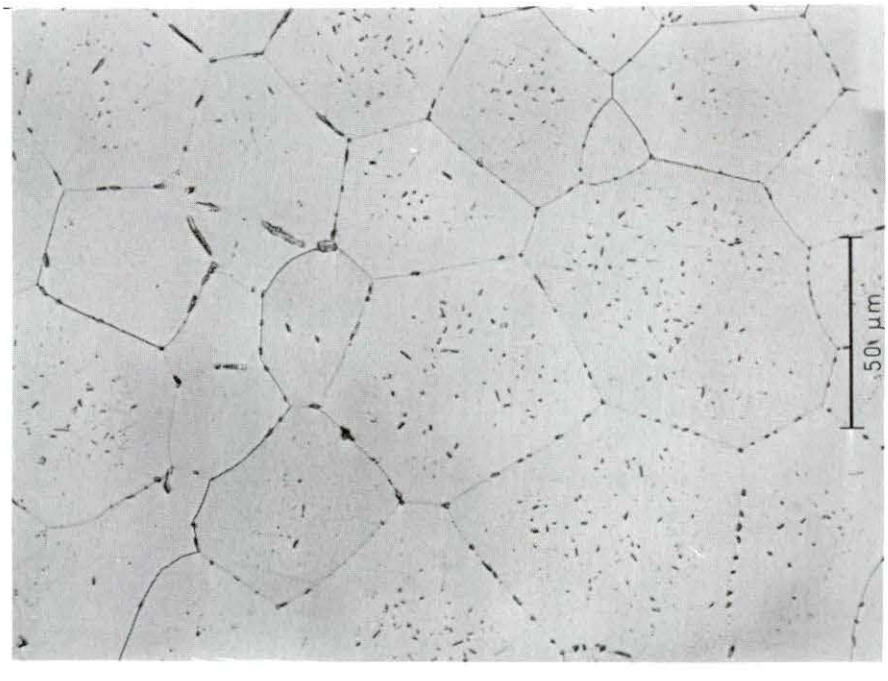

Metallograph 8: $La_{2.3}Eu_{0.7}S_4$ bottom of ingot vertical slice 500X.

Metallograph 9: $La_{2.7}Sm_{0.3}S_4$ top of ingot horizontal slice 500X.

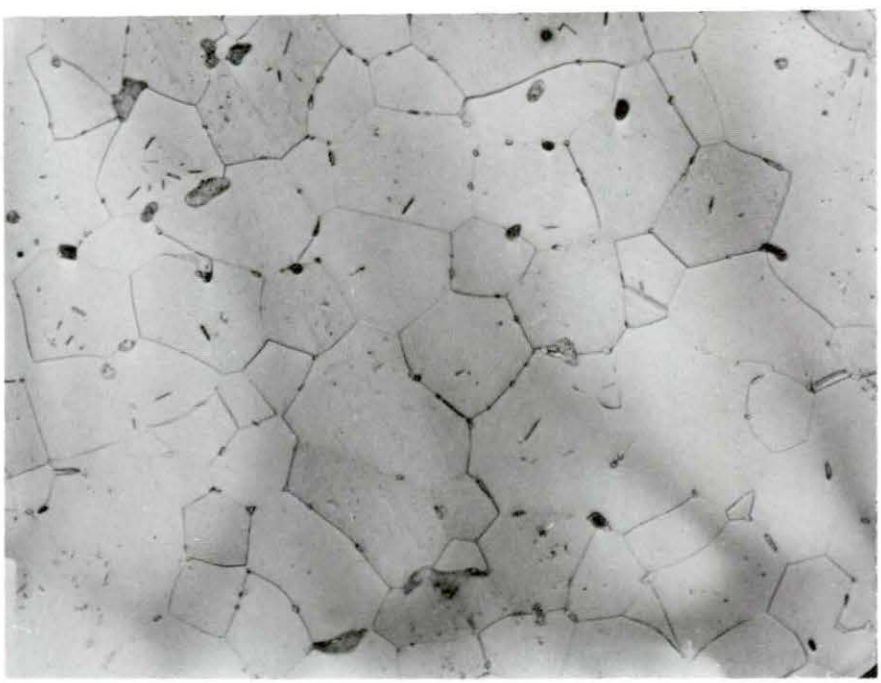

Metallograph 10: $La_{2.7}Sm_{0.3}S_4$ top of ingot vertical slice 500X.

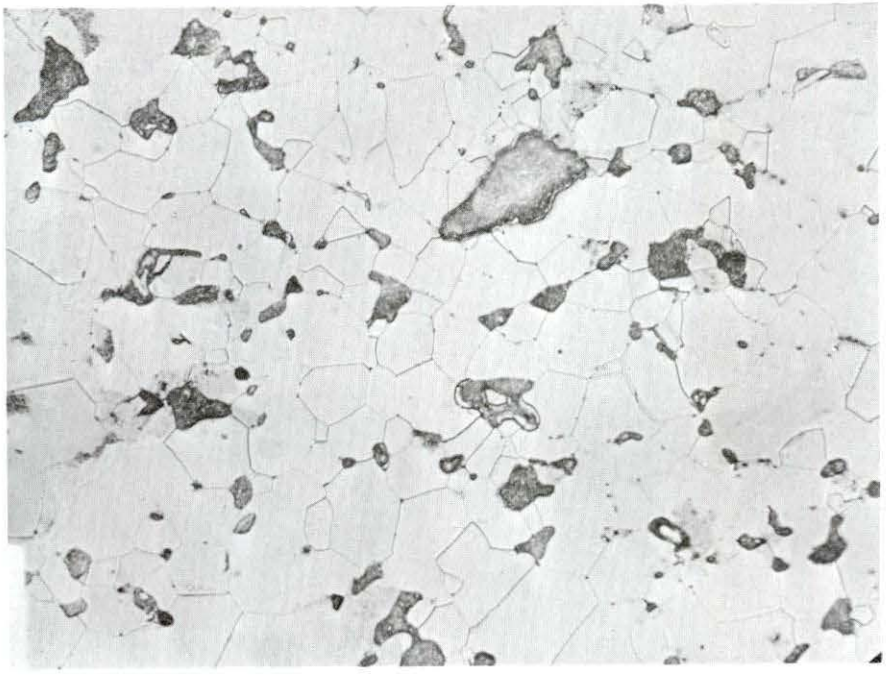

Metallograph 11: $La_{2.7}Sm_{0.3}S_4$ bottom of ingot horizontal slice 500X.

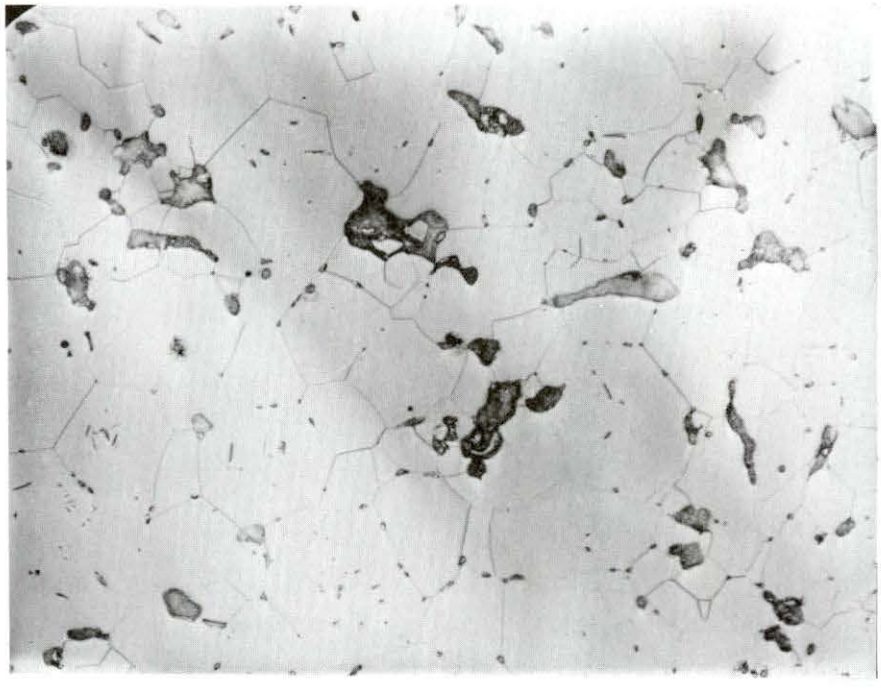

Metallograph 12: $La_{2.7}Sm_{0.3}S_4$ bottom of ingot vertical slice 500X.

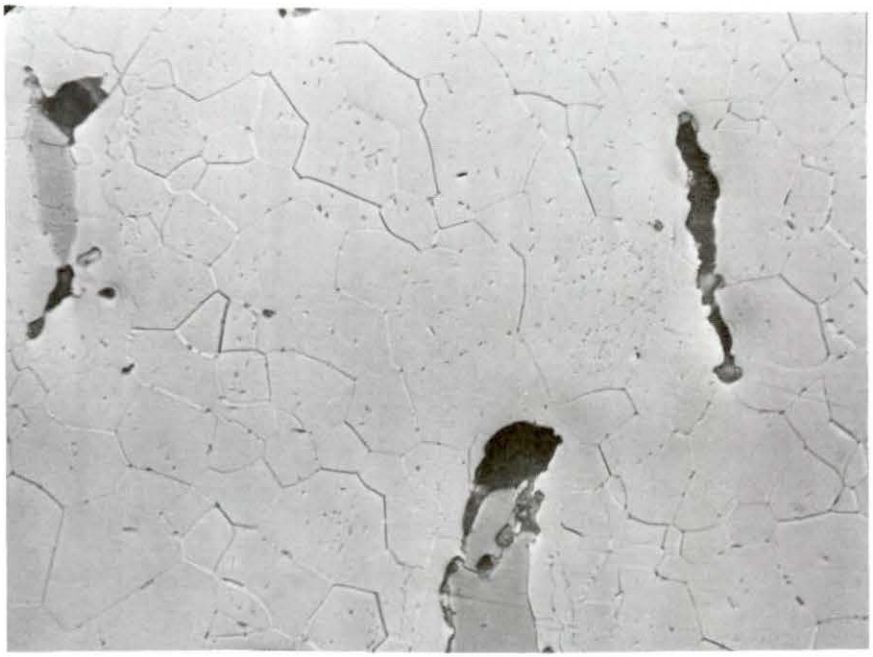

Metallograph 13: $La_{2.3}Sm_{0.7}S_4$ top of ingot horizontal slice 500X.

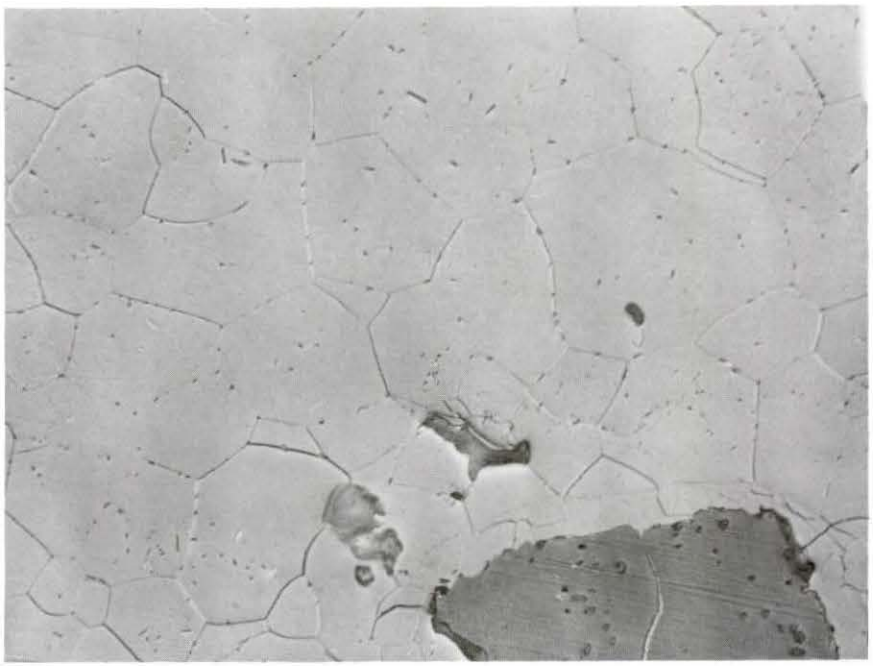

Metallograph 14: $La_{2.3}Sm_{0.7}S_4$ top of ingot vertical slice 500X.

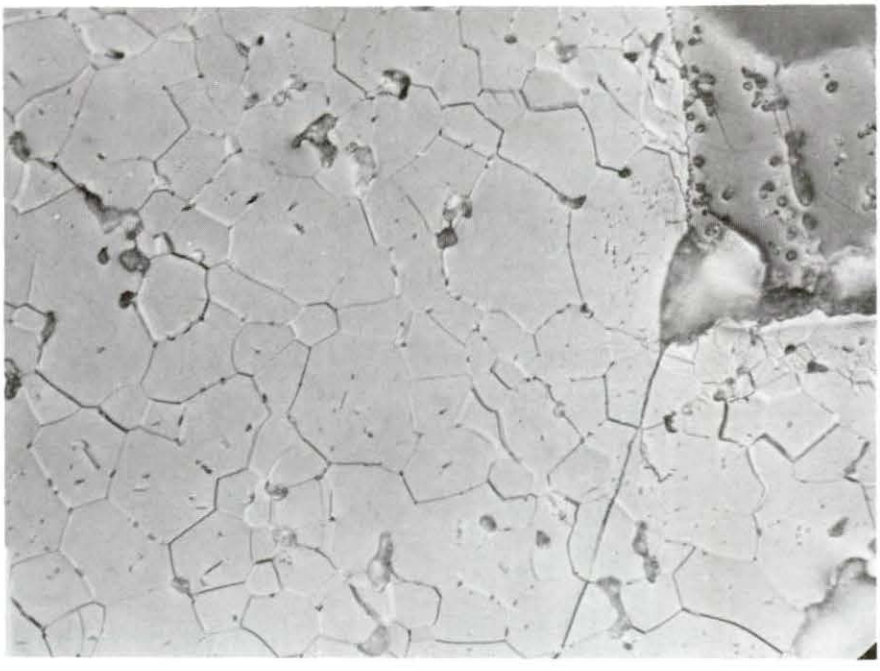

Metallograph 15: $La_{2.3}Sm_{0.7}S_4$ bottom of ingot horizontal slice 500X.

Metallograph 16: $La_{2.3}Sm_{0.7}S_4$ bottom of ingot vertical slice 500X.

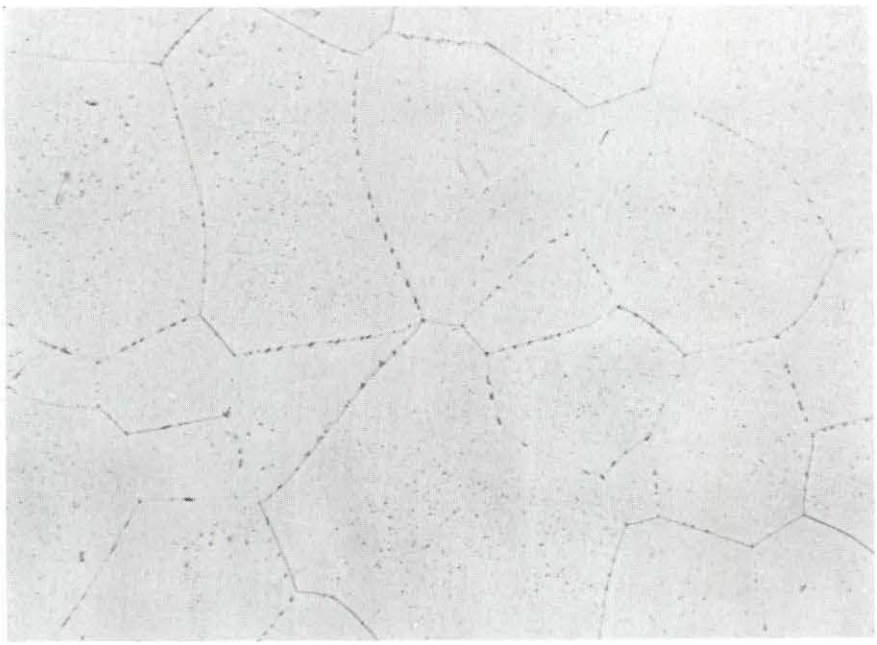

Metallograph 17: $La_{2.8}Yb_{0.2}S_4$ top of ingot horizontal slice 500X.

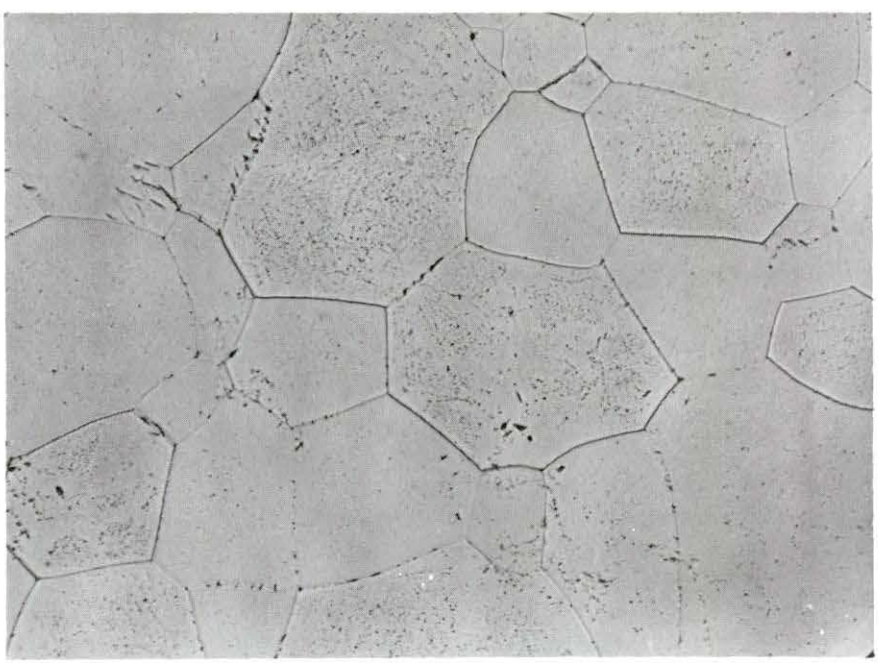

Metallograph 18: $La_{2.8}Yb_{0.2}S_4$ top of ingot vertical slice 500X.

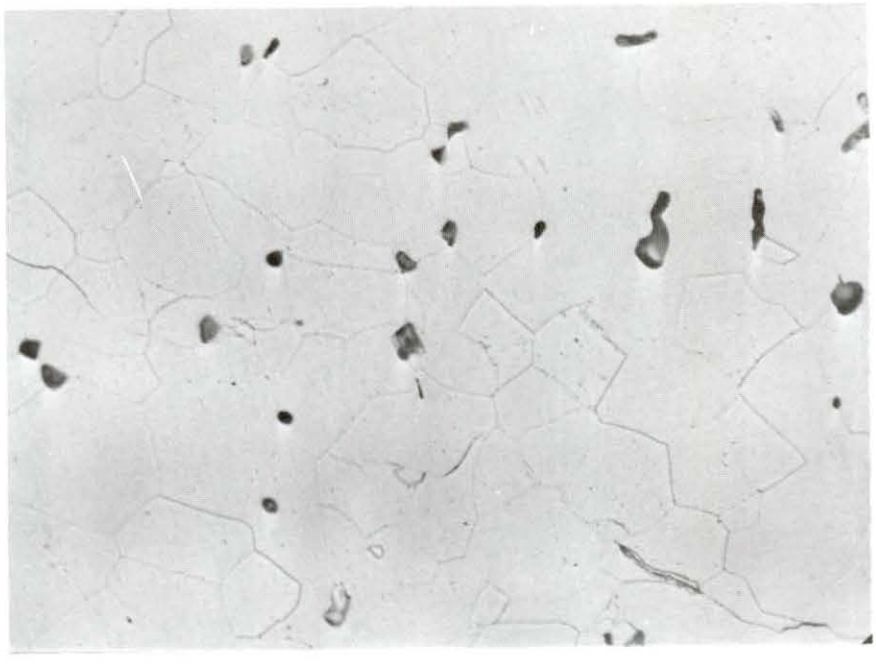

Metallograph 19: $La_{2.8}Yb_{0.2}S_4$ bottom of ingot horizontal slice 500X.

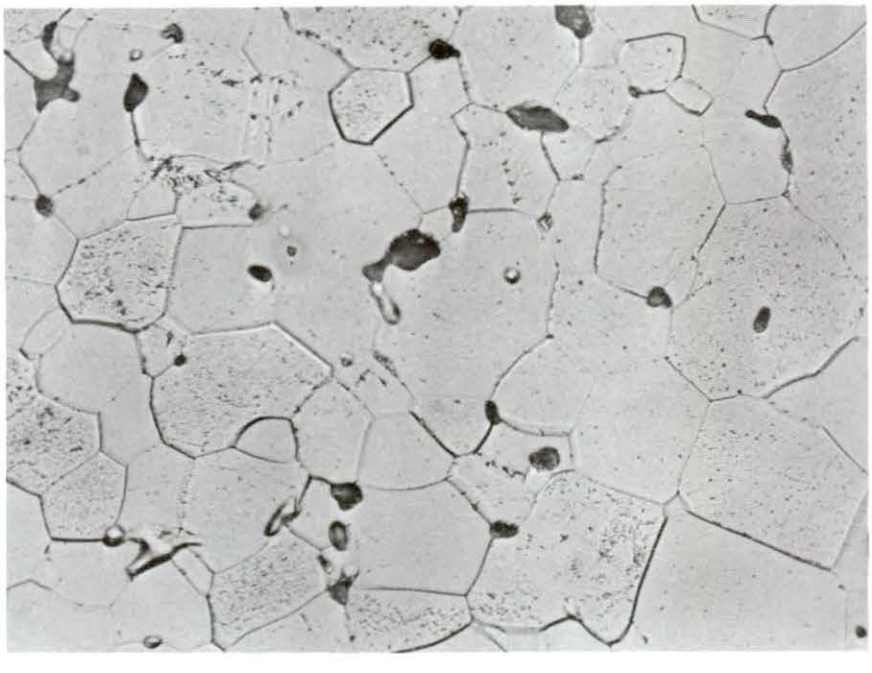

Metallograph 20: $La_{2.8}Yb_{0.2}S_4$ bottom of ingot vertical slice 500X.

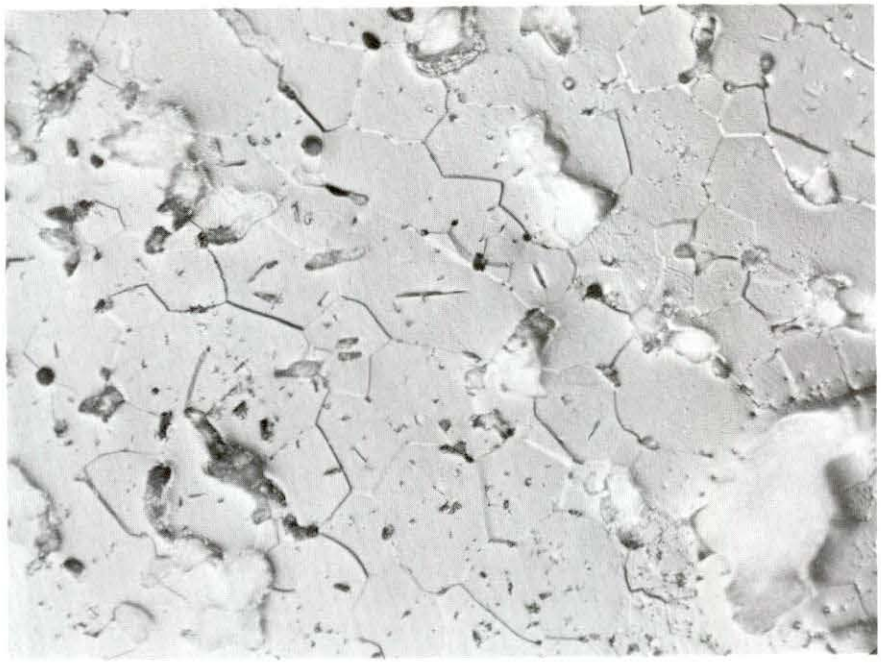

Metallograph 21: $La_{2.3}Yb_{0.7}S_4$ top of ingot horizontal slice 500X.

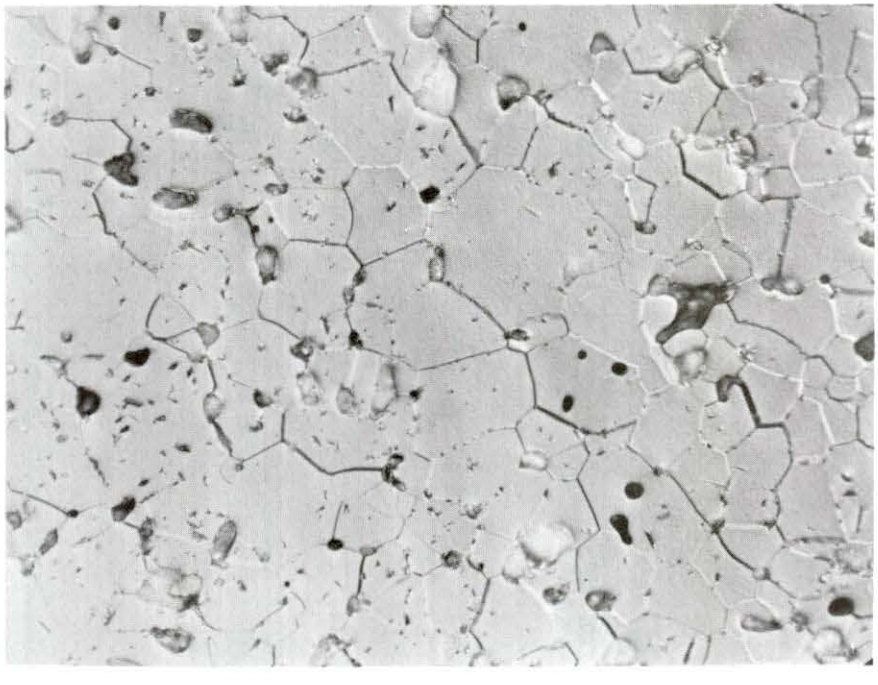

Metallograph 22: $La_{2.3}Yb_{0.7}S_4$ top of ingot vertical slice 500X.

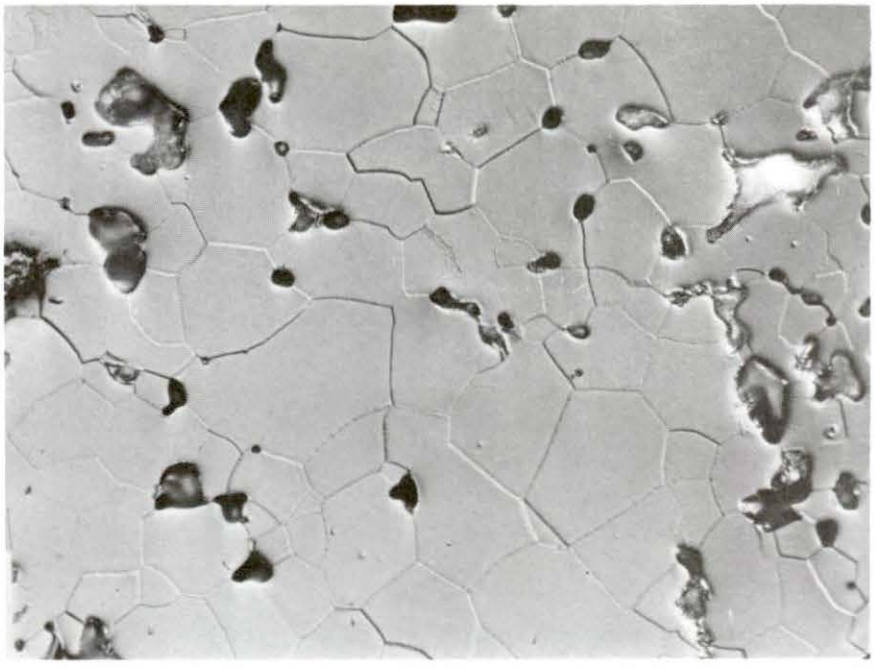

Metallograph 23: $La_{2.3}Yb_{0.7}S_4$ bottom of ingot horizontal slice 500X.

Metallograph 24: $La_{2.3}Yb_{0.7}S_4$ bottom of ingot vertical slice 500X.